REFORMULATED WEAK FORMULATION AND EFFICIENT FULLY DISCRETE FINITE ELEMENT METHOD FOR A TWO-PHASE FERROHYDRODYNAMICS SHLIOMIS MODEL*

GUO-DONG ZHANG[†], XIAOMING HE[‡], AND XIAOFENG YANG[§]

Abstract. The two-phase ferrohydrodynamics model consisting of Cahn-Hilliard equations, Navier-Stokes equations, magnetization equations, and magnetostatic equations is a highly nonlinear, coupled, and saddle point structural multiphysics PDE system. While various works exist to develop fully decoupled, linear, second-order in time, and unconditionally energy stable methods for simpler gradient flow models, existing ideas may not be applicable to this complex model or may be only applicable to part of this model. Therefore, significant challenges remain in developing corresponding efficient fully discrete numerical algorithms with the four above-mentioned desired properties, which will be addressed in this paper by dynamically incorporating several key ideas, including a reformulated weak formulation with special test functions for overcoming two major difficulties caused by the magnetostatic equation, the decoupling technique based on the "zeroenergy-contribution" property to handle the coupled nonlinear terms, the second-order projection method for the Navier-Stokes equations, and the invariant energy quadratization (IEQ) method for the time marching. Among all these ideas, the reformulated weak formulation serves as a key bridge between the existing techniques and the challenges of the target model, with all of the four desired properties kept in mind. We demonstrate the well-posedness of the proposed scheme and rigorously show that the scheme is unconditionally energy stable. Extensive numerical simulations, including accuracy/stability tests, and several 2D/3D benchmark Rosensweig instability problems for "spiking" phenomena of ferrofluids are performed to verify the effectiveness of the scheme.

Key words. ferrohydrodynamics, two-phase, fully decoupled, unconditional energy stability, second-order accuracy

MSC codes. 65N12, 65M12, 65M70

DOI. 10.1137/22M1499376

1. Introduction. Ferrofluids are colloidal suspensions formed by infusing small monodomain magnetic particles into a nonmagnetic carrier fluid. They have a "zero-magnetic-remanence" property; i.e., they can be magnetized by an external magnetic field, but their magnetization properties disappear completely in the absence of the applied magnetic field. This unique property enables ferrofluids to be widely used in many scientific and engineering fields requiring precise control, including assembly of micro-/nanoparticles [5, 11], ferrofluid jet [10, 19], fluid transport and control [34], sorting of biological cells [63], and microchannel flows [46]. Two versions of

^{*}Submitted to the journal's Computational Methods in Science and Engineering section May 31, 2022; accepted for publication (in revised form) December 29, 2022; published electronically June 1, 2023.

https://doi.org/10.1137/22M1499376

Funding: The first author's research partially supported by the National Science Foundation of China under grants 12171415 and 12271468. The second author's research was partially supported by the U.S. National Science Foundation under grant DMS-1818642. The third author's research partially supported by the U.S. National Science Foundation under grants DMS-1818783 and DMS-2012490.

[†]School of Mathematics and Information Sciences, Yantai University, Yantai, 264005, Shandong, People's Republic of China (gdzhang@ytu.edu.cn).

[‡]Department of Mathematics, Missouri University of Science & Technology, Rolla, MO 65409 USA (hex@mst.edu).

 $^{^\}S$ Corresponding author. Department of Mathematics, University of South Carolina, Columbia, SC 29208 USA (xfyang@math.sc.edu).

mathematical models describing ferrohydrodynamics (FHD) were originally developed by Rosensweig (cf. [37, 38]) and Shliomis (cf. [48, 49]), respectively. The two models have both similarities and differences. For example, they both treat ferrofluid as a homogeneous single-phase fluid. But they are quite different in explaining the motion of particles. For example, the Rosensweig model establishes a partial differential equation of the angular velocity to calculate the spin of nanoparticles, while the Shliomis model treats the spin as a magnetic torque. Recently, both of these models have been applied to solve engineering applications involving two-phase ferrofluid models (one phase has magnetic properties and the other does not), such as magnetic manipulation of microchannel flows [27, 32], microvalves [30, 50], drag targeted therapy [31, 47], magnetically guided transport [1], etc.

In recent years, the phase-field type model has been extensively applied to simulate multiphase fluid flow systems. Due to the high stiffness it carries, the model provides a formidable challenge to the design of numerical methods, where numerical approaches satisfying energy stability are recognized as being more effective for solving the model [29, 62]. Existing numerical methodologies include the convex-splitting strategy [3, 7, 20, 21, 26, 36, 40, 53], the stabilization method [13, 14, 23, 44, 52], the invariant energy quadratization approach [9, 51, 58, 59, 60, 61, 67], the scalar auxiliary variable approach [2, 7, 12, 15, 25, 28, 35, 41], and the zero-energy-contribution framework [54, 55, 56, 57, 64, 66]. The FHD system, which is a specific instance of a multiphase flow system, is also being modeled using the phase-field method, and some initial progress has been made in algorithm design and simulation.

However, to the best of the authors' knowledge, the current work on numerical algorithm development and analysis of two-phase FHD models is still in its infancy, especially for models constructed using the phase-field (diffusive-interface) method. In the pioneering work of [33], the authors used the phase-field method to establish a two-phase ferrofluid mathematical model coupling the monophase Shliomis model and the Cahn-Hilliard equation. The authors also proposed an unconditionally energy stable scheme and proved the convergence. The numerical algorithm developed in [33] is the first energy stable scheme for the two-phase FHD model, which lays a solid foundation for the development of numerical methods for the phase-field type FHD model. However, the numerical scheme developed in [33] is nonlinear, coupled, and first-order accurate in time, and the space is discretized by using the hybrid finite element discretizations (discontinuous and continuous finite element discretizations are combined). Recently, a linear, decoupled, unconditionally energy stable scheme has been developed in [65] where the space is discretized by using the continuous finite element method, which is simpler to implement. However, the scheme in [65] is still of first-order temporal accuracy and partially decoupled. Also, the numerical experiments in both [33, 65] are limited to two dimensions. Furthermore, even though the magnetostatic equation looks like the easiest equation in the whole system, the fact is quit the opposite, and it actually caused two major drawbacks of the algorithm in [65]. One is a stability problem when one tries to decouple the magnetic potential from the magnetization, which is actually the reason why the scheme in [65] is not fully decoupled. The other one is the introduction of an auxiliary variable when one tries to use continuous finite elements instead of discontinuous Galerkin for the magnetization equation.

Therefore, in this paper, our goal is to develop a fully discrete numerical scheme with second-order time accuracy, linearity, unconditional energy stability, and fully decoupled structure based on the continuous finite element method and also perform simulations in both two and three dimensions. Meanwhile, we will also overcome the

above two drawbacks caused by the magnetostatic equation in [65]. To achieve these goals, we incorporate the following five key ideas.

First, to decouple the magnetic potential from the magnetization, we reformulate the weak formulation of the magnetostatic equation by combining some special structural features of the magnetostatic equation and the magnetization equation. Specifically, we test appropriately chosen functions on the magnetostatic equation, its temporal derivative equation, and the magnetization equation. Then we combine the resulted equations to cancel the original coupling term in the magnetostatic equation and derive a new equivalent weak formulation with several extra terms. This reconstruction not only helps us to achieve fully decoupled structures but also enables us to naturally apply the continuous finite element method to discretize the magnetization equations, rather than introducing an auxiliary magnetic field in continuous finite element space as in [65] or using the discontinuous finite element method as in [33].

Second, to further decouple the magnetic fields, flow field, and phase-field variable completely while maintaining the unconditional energy stability, we adopt the recently developed decoupling framework using a nonlocal scalar auxiliary variable for the nonlinear coupling terms satisfying the so-called "zero-energy-contribution" feature; see [54, 55]. The key idea is to further reformulate the system into an equivalent form coupled with some special ordinary differential equation (ODE) consisting of those terms satisfying the "zero-energy-contribution" feature. The main motivation for defining a nonlocal variable and developing an equivalent system is that the unconditional stability and fully decoupled linearized structure can be simultaneously obtained by explicit treatments of nonlinear terms. More importantly, under this fully decoupled linearized structure of unconditional stability, this idea provides a great chance to achieve second-order accuracy for temporal discretization. This is a well-known challenge in the efficiency, accuracy, and stability of numerical methods for this type of sophisticated model, for which the extra cost paid in the above two intermediate reformulations is worthwhile. The design of the particular ODE is entirely dependent on the characteristics of the model. Hence its design requires careful consideration, especially when the model studied in this paper is very complex, involving many complicated nonlinear terms coupled to the magnetic, magnetization, and velocity fields

Third, two critical ideas will be utilized to deal with three nonlinear terms obtained from the above first reformulated model in an efficient way. On one hand, two nonlinear terms happen to satisfy the "zero-energy-contribution" characteristic and hence can also be naturally incorporated in the nonlocal scalar variable Q. This is another major difference from the existing works on constructing the ODE for Q. On the other hand, since the third nonlinear term possesses a positive definite structure, it can be decoupled by an appropriate two-step implicit-explicit scheme while maintaining unconditional stability.

Fourth, we use the second-order accurate projection method [18, 39] to decouple the calculation of the pressure from the momentum equation.

Fifth, the nonlinear double-well potential contained in the phase-field equation is treated by using the recently developed invariant energy quadratization (IEQ) method (cf. [59, 60]) to ensure the unconditional energy stability, second-order temporal accuracy, and linearity.

With the ideas described above, we construct a desired efficient scheme, which is a continuous finite element scheme and has the characteristics of fully decoupling, second-order accuracy in time, unconditional energy stability, and linearity. These advantages are our main motivation to reconstruct the original model at the cost

of constructing a more complex (but equivalent) formalism. The final numerical implementation of the reconstructed model only requires the solution of several independent elliptic equations without increasing the computational complexity of the final algorithm at all. It is worthwhile to concentrate on the process of reformulation to improve the stability, efficiency, and accuracy of the numerical implementation of such complex models. In addition, the developed algorithm transforms the nonlinear coupled, saddle-point structure multiphysics two-phase FHD problem into multiple independent elliptic type problems, resulting in a very convenient solution process. We further establish the well-posedness of the proposed scheme and rigorously prove the unconditional energy stability. Through various numerical simulations, including the accuracy test, energy stability verification, and some 2D/3D benchmark problems, the effectiveness of the proposed scheme is verified, and some iconic "spiking" phenomena of two-phase ferrofluid are simulated. To the best of the authors' knowledge, the developed scheme is the first second-order accurate in time and fully decoupled scheme for the two-phase FHD phase-field model.

We organize the rest of the article in the following way. In section 2, we present the two-phase FHD phase-field model and reformulate it as an equivalent weak form that facilitates numerical discretization. In section 3, we construct our numerical scheme and prove its unconditional energy stability and well-posedness. In section 4, we present various 2D and 3D numerical simulations to verify the effectiveness of the scheme. Some concluding remarks are made in section 5.

2. Two-phase FHD phase-field system and its energy law.

2.1. The two-phase FHD model. Let $\Omega \subset \mathbb{R}^d$ with d=2 or 3 be a bounded convex polygon or polyhedron domain. The Shliomis model for a viscous, homogeneous, nonconducting ferrofluid flow system reads as follows [33, 49]:

$$(2.1) \begin{cases} \boldsymbol{u}_{t} - \nu \Delta \boldsymbol{u} + (\boldsymbol{u} \cdot \nabla) \boldsymbol{u} + \nabla p = \mu(\boldsymbol{m} \cdot \nabla) \boldsymbol{h} + \frac{\mu}{2} \nabla \times (\boldsymbol{m} \times \boldsymbol{h}), \\ \nabla \cdot \boldsymbol{u} = 0, \\ \boldsymbol{m}_{t} + (\boldsymbol{u} \cdot \nabla) \boldsymbol{m} - \frac{1}{2} \nabla \times \boldsymbol{u} \times \boldsymbol{m} = -\frac{1}{\tau} (\boldsymbol{m} - \chi_{0} \boldsymbol{h}) - \beta \boldsymbol{m} \times (\boldsymbol{m} \times \boldsymbol{h}), \\ - \Delta \varphi = \nabla \cdot (\boldsymbol{m} - \boldsymbol{h}_{a}), \\ \boldsymbol{u}|_{\partial \Omega} = \boldsymbol{0}, \quad \partial_{n} \varphi|_{\partial \Omega} = (\boldsymbol{h}_{a} - \boldsymbol{m}) \cdot \boldsymbol{n}_{\partial \Omega}, \quad \boldsymbol{u}(0, \boldsymbol{x}) = \boldsymbol{u}_{0}, \quad \boldsymbol{m}(0, \boldsymbol{x}) = \boldsymbol{m}_{0}. \end{cases}$$

Here \boldsymbol{u} is the velocity field, p is the pressure, \boldsymbol{m} is the magnetization field, $\boldsymbol{h}(:=\nabla\varphi)$ is the effective magnetic field, φ is the magnetic potential, \boldsymbol{h}_a is a smooth harmonic applied magnetic field $(\nabla \times \boldsymbol{h}_a = \boldsymbol{0}, \nabla \cdot \boldsymbol{h}_a = 0)$, ν is the kinematic fluid viscosity, χ_0 is magnetic susceptibility, μ is permeability of free space, τ is relaxation time constant, $\beta = \frac{1}{6\nu\vartheta}$, ϑ is volume fraction of dispersed solid phase, $\boldsymbol{n}_{\vartheta\Omega}$ is the outward normal on the boundary $\partial\Omega$, and the term $(\boldsymbol{m}\cdot\nabla)\boldsymbol{h}$ is the so-called Kelvin force.

In the framework of the phase-field approach, to simulate the immiscible mixture consisting of the ferrofluid and nonferromagnetic viscous fluid, a labeling variable Φ is defined as

$$\Phi(t, \boldsymbol{x}) = \begin{cases} 1 & \text{ferrofluid phase,} \\ 0 & \text{nonferromagnetic viscous fluid} \end{cases}$$

with a thin smooth transition layer of thickness ϵ connecting the two fluids. Then the interface of the mixture can be recorded using $\Gamma = \{x : \Phi(t, x) = 1/2\}$. We assume that the evolution of the phase-field variable follows the Cahn–Hilliard dynamics that read as

(2.2)
$$\begin{cases} \Phi_t + \nabla \cdot (\boldsymbol{u}\Phi) = M\Delta W, \\ W = -\lambda \epsilon \Delta \Phi + \lambda f(\Phi), \\ \Phi(0, \boldsymbol{x}) = \Phi_0, \quad \partial_n \Phi|_{\partial\Omega} = 0, \quad \partial_n W|_{\partial\Omega} = 0, \end{cases}$$

where M>0 is the mobility parameter, W is the chemical potential, λ accounts as the surface tension parameter, and $f(\Phi)=F'(\Phi),\ F(\Phi)=\frac{1}{4\epsilon}\Phi^2(\Phi-1)^2$ is the Ginzburg–Landau double-well potential.

The two-phase FHD model coupling the Shiliomis model (2.1) and the Cahn–Hilliard system (2.2) are given as follows (cf. the detailed modeling work given in [33, 49, 65]):

- $(2.3) \quad \Phi_t + \nabla \cdot (\boldsymbol{u}\Phi) = M\Delta W,$
- (2.4) $W = -\lambda \epsilon \Delta \Phi + \lambda f(\Phi),$
- $(2.5) \quad \boldsymbol{u}_{t} \nabla \cdot \nu(\Phi)D(\boldsymbol{u}) + (\boldsymbol{u} \cdot \nabla)\boldsymbol{u} + \nabla p + \Phi \nabla W = \mu(\boldsymbol{m} \cdot \nabla)\boldsymbol{h} + \frac{\mu}{2}\nabla \times (\boldsymbol{m} \times \boldsymbol{h}),$
- $(2.6) \quad \nabla \cdot \boldsymbol{u} = 0,$

(2.7)
$$m_t + (\boldsymbol{u} \cdot \nabla) \boldsymbol{m} - \frac{1}{2} \nabla \times \boldsymbol{u} \times \boldsymbol{m} + \beta \boldsymbol{m} \times (\boldsymbol{m} \times \boldsymbol{h}) = -\frac{1}{\tau} (\boldsymbol{m} - \chi(\Phi) \boldsymbol{h}),$$

- $(2.8) \quad -\Delta\varphi = \nabla \cdot (\boldsymbol{m} \boldsymbol{h}_a),$
- $(2.9) \quad \partial_n \Phi|_{\partial\Omega} = 0, \quad \partial_n W|_{\partial\Omega} = 0, \quad \boldsymbol{u}|_{\partial\Omega} = \boldsymbol{0}, \quad \partial_n \varphi|_{\partial\Omega} = (\boldsymbol{h}_a \boldsymbol{m}) \cdot \boldsymbol{n}_{\partial\Omega}.$
- (2.10) $\Phi(0, \mathbf{x}) = \Phi_0$, $\mathbf{u}(0, \mathbf{x}) = \mathbf{u}_0$, $\mathbf{m}(0, \mathbf{x}) = \mathbf{m}_0$.

Here $\nu(\Phi) = \nu_w + (\nu_f - \nu_w) \frac{1}{1 + e^{-(2\Phi - 1)/\epsilon}}$, ν_f and ν_w are viscosities for the ferrofluid phase and nonferromagnetic viscous mediums, respectively, $\chi(\Phi) = \chi_0 \frac{1}{1 + e^{-(2\Phi - 1)/\epsilon}}$ (another choice of $\chi(\Phi) = \Phi^2 \chi_0$ can also be used for simplicity), $D(\boldsymbol{u}) = \frac{1}{2} (\nabla \boldsymbol{u} + (\nabla \boldsymbol{u})')$, and the term $\Phi \nabla W$ is the induced elastic stress by the mixing energy [33, 43, 44].

Hereafter, for two vector functions $\boldsymbol{x}, \boldsymbol{y}$, we denote the L^2 inner product as $(\boldsymbol{x}, \boldsymbol{y}) = \int_{\Omega} \boldsymbol{x} \cdot \boldsymbol{y} dx$ and L^2 -norm $\|\boldsymbol{x}\|^2 = (\boldsymbol{x}, \boldsymbol{x})$. We use $H^1(\Omega)$ to denote the usual Sobolev space, and we define $H^1_0(\Omega) = \{\phi \in H^1(\Omega) : \phi|_{\partial\Omega} = 0\}$, $L^2_0(\Omega) = \{\phi \in L^2(\Omega) : \int_{\Omega} \phi dx = 0\}$, $H^1(\Omega) = H^1(\Omega)^d$, and $H^1_0(\Omega) = H^1_0(\Omega)^d$.

The two-phase FHD system (2.3)–(2.10) satisfies the following energy stability/dissipation law.

LEMMA 2.1 (Theorem 2.1 in [65]). Assuming $\chi(\Phi) \leq \chi_0$, the system (2.3)–(2.10) satisfies the following energy stability:

$$\frac{d}{dt}E(\Phi, \boldsymbol{u}, \boldsymbol{h}, \boldsymbol{m}) + D(W, \boldsymbol{u}, \boldsymbol{h}, \boldsymbol{m}) \le \frac{\mu}{\tau} \|\boldsymbol{h}_a\|^2 + \tau \mu \|\boldsymbol{h}_b\|^2,$$

where $\mathbf{h}_b = \partial_t \mathbf{h}_a$ and

$$(2.11) E(\Phi, \boldsymbol{u}, \boldsymbol{h}, \boldsymbol{m}) = \lambda \left(\frac{\epsilon}{2} \|\nabla \Phi\|^2 + (F(\Phi), 1) \right) + \frac{1}{2} \|\boldsymbol{u}\|^2 + \frac{\mu}{2} \|\boldsymbol{h}\|^2 + \frac{\mu}{2\chi_0} \|\boldsymbol{m}\|^2,$$

(2.12)
$$D(W, \boldsymbol{u}, \boldsymbol{h}, \boldsymbol{m}) = M \|\nabla W\|^2 + \|\sqrt{\nu(\Phi)}D(\boldsymbol{u})\|^2 + \frac{\mu}{2\tau}\|\boldsymbol{h}\|^2 + \mu\beta\|\boldsymbol{m} \times \boldsymbol{h}\|^2 + \frac{3\mu}{4\tau\chi_0}\|\boldsymbol{m}\|^2.$$

For the case of no applied magnetic field $(\mathbf{h}_a = \mathbf{0})$, the following energy dissipation law holds:

$$\frac{d}{dt}E(\Phi, \boldsymbol{u}, \boldsymbol{h}, \boldsymbol{m}) + D(W, \boldsymbol{u}, \boldsymbol{h}, \boldsymbol{m}) \le 0.$$

Remark 2.1. Normally the magnetostatic equation (2.8) seems to be very simple, and its solvability is taken for granted. However, this equation poses two unexpected difficulties in designing numerical methods, especially when a numerical scheme with a decoupled structure is expected. First, note that there exists a linear coupling between the magnetic potential φ and magnetization field m, and it is difficult to decouple them under the premise of unconditional stability. This leads to the coupled type scheme developed in [33, 65]. Second, the definition of $h = \nabla \varphi$ implies that if a direct implicit discretization is adopted for (2.8), a hybrid finite element method is required, e.g., the discontinuous Galerkin method for h and the continuous Galerkin method for φ (see [33]), which is not easy to implement as well. Or one may adopt the indirect discretization method, such as introducing one auxiliary magnetic variable h (see the details in our previous work [65]), which makes it possible to use the continuous finite element method. However, the indirect discretization can only achieve first-order accuracy in time. In the following subsections, we will perform a new reformulation of the magnetostatic equation (2.8) to obtain an equivalent form, which facilitates the simultaneous development of schemes with decoupling structure and second-order time accuracy.

2.2. Reformulated formulation. To facilitate the design of numerical algorithms, we convert the system (2.3)–(2.10) into an equivalent form.

First, we deal with the magnetic potential equation (2.8) by constructing its weak form: find $\varphi \in H^1(\Omega) \cap L^2_0(\Omega)$, such that

$$(2.13) \qquad \frac{1}{\tau}(\nabla\varphi,\nabla\psi) + \frac{1}{\tau}(\boldsymbol{m},\nabla\psi) = \frac{1}{\tau}(\boldsymbol{h}_a,\nabla\psi) \ \forall \psi \in H^1(\Omega) \cap L^2_0(\Omega).$$

By taking the time derivative of (2.8) and formulating the obtained equation in the weak form, we obtain

(2.14)
$$(\nabla \varphi_t, \nabla \psi) + (\boldsymbol{m}_t, \nabla \psi) = (\boldsymbol{h}_b, \nabla \psi).$$

By taking the L^2 inner product of the magnetization equation (2.7) with $\nabla \psi$, we derive

$$(2.15)$$

$$\frac{1}{\tau}(\chi(\Phi)\nabla\varphi,\nabla\psi) - ((\boldsymbol{u}\cdot\nabla)\boldsymbol{m},\nabla\psi) + \frac{1}{2}(\nabla\times\boldsymbol{u}\times\boldsymbol{m},\nabla\psi) + \beta(\boldsymbol{m}\times\nabla\varphi,\boldsymbol{m}\times\nabla\psi)$$

$$= (\boldsymbol{m}_t,\nabla\psi) + \frac{1}{\tau}(\boldsymbol{m},\nabla\psi).$$

Summing up (2.13)–(2.15), we get a new magnetostatic equation which will be used to replace (2.8) and reads as

$$\begin{aligned} (\nabla \varphi_t, \nabla \psi) + \frac{1}{\tau} (\nabla \varphi, \nabla \psi) + \frac{1}{\tau} (\chi(\Phi) \nabla \varphi, \nabla \psi) + \beta (\boldsymbol{m} \times \nabla \varphi, \boldsymbol{m} \times \nabla \psi) - ((\boldsymbol{u} \cdot \nabla) \boldsymbol{m}, \nabla \psi) \\ (2.16) \\ + \frac{1}{2} (\nabla \times \boldsymbol{u} \times \boldsymbol{m}, \nabla \psi) = \frac{1}{\tau} (\boldsymbol{h}_a, \nabla \psi) + (\boldsymbol{h}_b, \nabla \psi). \end{aligned}$$

Remark 2.2. The above reconstruction process gives us a new magnetostatic equation (2.16) that appears to be more complex than the original magnetostatic equation (2.8). In practice, however, the new magnetostatic equation (2.16) actually makes it easier for us to design numerical schemes with unconditional stability and a fully decoupled structure for the following two reasons:

- First, in (2.16), the linear coupling of magnetic potential φ and magnetization \boldsymbol{m} disappears, thus offering the possibility to develop a fully decoupled algorithm. Although several nonlinear terms appear, e.g., the two terms $\frac{1}{2}(\nabla \times \boldsymbol{u} \times \boldsymbol{m}, \nabla \psi) ((\boldsymbol{u} \cdot \nabla)\boldsymbol{m}, \nabla \psi)$, they actually satisfy the property of "zero-energy-contribution." Hence they can be decoupled by applying the decoupling technique through the nonlocal auxiliary variable; see the details in section 2.3. Another additional nonlinear coupling term $\beta(\boldsymbol{m} \times \nabla \varphi, \boldsymbol{m} \times \nabla \psi)$ does not satisfy the "zero-energy-contribution" property, but note that it owns the positive definite structure. Therefore, it can be handled by the two-step implicit-explicit discretization to achieve the decoupling calculation; see section 3.2.
- Second, the disappearance of the linear coupling between the magnetic potential φ and the magnetization \boldsymbol{m} allows us to apply the continuous finite element method to solve (2.7) and (2.16). Therefore, it is not necessary to use discontinuous finite elements for \boldsymbol{m} as [33], nor to introduce additional auxiliary variable $\tilde{\boldsymbol{h}}$ as [65].

Second, we apply the IEQ method $[59,\,60]$ to recast the Cahn–Hilliard equation. Denote

$$U = \sqrt{F(\Phi) - \frac{S}{2\epsilon}\Phi^2 + B}, \quad H(\Phi) = \frac{f(\Phi) - \frac{S}{\epsilon}\Phi}{\sqrt{F(\Phi) - \frac{S}{2\epsilon}\Phi^2 + B}},$$

where S is an adjustable positive parameter that works as a stabilization term (see Remark 2.4), and B is a chosen constant such that $F(\Phi) - \frac{S}{2\epsilon}\Phi^2 + B > 0$. With these formulas, we obtain the equivalent phase-field equations as follows:

$$\Phi_t + \nabla \cdot (\boldsymbol{u}\Phi) = M\Delta W, \quad W = -\lambda \epsilon \Delta \Phi + \lambda H(\Phi) U + \frac{S\lambda}{\epsilon} \Phi, \quad U_t = \frac{1}{2} H(\Phi) \Phi_t.$$

The corresponding weak form can be written as follows: find $\Phi \in H^1(\Omega)$, $W \in H^1(\Omega)$ such that for all $\Lambda \in H^1(\Omega)$, $X \in H^1(\Omega)$, the following hold:

(2.17)
$$(\Phi_t, \Lambda) - (\boldsymbol{u}\Phi, \nabla\Lambda) = -M(\nabla W, \nabla\Lambda),$$

$$(W,X) = \lambda \epsilon(\nabla \Phi, \nabla X) + \lambda(H(\Phi)U,X) + \frac{S\lambda}{\epsilon}(\Phi,X),$$

$$(2.19) U_t = \frac{1}{2}H(\Phi)\Phi_t.$$

Third, we recast the Kelvin force term in the momentum equation (2.5). By taking the L^2 inner product of (2.5) with a test function $\mathbf{v} \in \mathbf{H}_0^1(\Omega)$, the Kelvin force term becomes $\mu((\mathbf{m} \cdot \nabla)\mathbf{h}, \mathbf{v})$. Since $\mathbf{h} = \nabla \varphi$, this term will bring boundary integrations involving jump and average terms across interior boundaries when applying the finite element method for spatial discretization; cf. [33]. We solve this issue by rewriting this term as

$$(2.20) \quad \mu((\boldsymbol{m}\cdot\nabla)\boldsymbol{h},\boldsymbol{v}) = \mu((\boldsymbol{v}\cdot\nabla)\boldsymbol{h},\boldsymbol{m}) = -\mu((\boldsymbol{v}\cdot\nabla)\boldsymbol{m},\boldsymbol{h}) - \mu((\nabla\cdot\boldsymbol{v})\boldsymbol{m},\boldsymbol{h}),$$

where the fact that $\nabla \times \mathbf{h} = 0$ and integration by parts are used. In this way, first-order spatial derivatives only exert on \mathbf{v} , \mathbf{m} , φ in (2.20), instead of \mathbf{h} .

From (2.20), we obtain the weak form of (2.5)–(2.6) that reads as follows: find $\mathbf{u} \in \mathbf{H}_0^1(\Omega)$, $p \in L_0^2(\Omega)$, such that for all $\mathbf{v} \in \mathbf{H}_0^1(\Omega)$, $q \in L_0^2(\Omega)$, the following hold:

$$(2.21) (\boldsymbol{u}_t, \boldsymbol{v}) + (\nu(\Phi)D(\boldsymbol{u}), D(\boldsymbol{v})) + ((\boldsymbol{u} \cdot \nabla)\boldsymbol{u}, \boldsymbol{v}) - (p, \nabla \cdot \boldsymbol{v}) + (\Phi\nabla W, \boldsymbol{v})$$

$$= -\mu((\boldsymbol{v} \cdot \nabla)\boldsymbol{m}, \boldsymbol{h}) - \mu((\nabla \cdot \boldsymbol{v})\boldsymbol{m}, \boldsymbol{h}) + \frac{\mu}{2}(\boldsymbol{m} \times \boldsymbol{h}, \nabla \times \boldsymbol{v}),$$
(2.22)
$$(\nabla \cdot \boldsymbol{u}, q) = 0.$$

Fourth, by applying the test function $n \in H^1(\Omega)$ for (2.7), we obtain

(2.23)
$$(\boldsymbol{m}_{t}, \boldsymbol{n}) + ((\boldsymbol{u} \cdot \nabla)\boldsymbol{m}, \boldsymbol{n}) - \frac{1}{2}(\nabla \times \boldsymbol{u} \times \boldsymbol{m}, \boldsymbol{n})$$
$$-\beta(\boldsymbol{m} \times \boldsymbol{h}, \boldsymbol{m} \times \boldsymbol{n}) + \frac{1}{\tau}(\boldsymbol{m}, \boldsymbol{n}) = \frac{1}{\tau}(\chi(\Phi)\boldsymbol{h}, \boldsymbol{n}).$$

Finally, by combining (2.16), (2.17)–(2.19), (2.21)–(2.22), and (2.23), we obtain a reformulated equivalent system in the weak form that reads as follows: find $(\Phi, W) \in H^1(\Omega)^2$, $\boldsymbol{u} \in \boldsymbol{H}^1(\Omega)$, $p \in L^2_0(\Omega)$, $\varphi \in H^1(\Omega) \cap L^2_0(\Omega)$, $\boldsymbol{m} \in \boldsymbol{H}^1(\Omega)$, such that for all $(\Lambda, X) \in H^1(\Omega)^2$, $\boldsymbol{v} \in \boldsymbol{H}^1(\Omega)$, $q \in L^2_0(\Omega)$, $\psi \in H^1(\Omega) \cap L^2_0(\Omega)$, $\boldsymbol{n} \in \boldsymbol{H}^1(\Omega)$, the following hold:

(2.24)

$$(\Phi_t, \Lambda) - (\boldsymbol{u}\Phi, \nabla\Lambda) = -M(\nabla W, \nabla\Lambda),$$

(2.25)

$$(W,X) = \lambda \epsilon(\nabla \Phi, \nabla X) + \lambda (H(\Phi)U, X) + \frac{S\lambda}{\epsilon} (\Phi, X),$$

(2.26)

$$U_t = \frac{1}{2}H(\Phi)\Phi_t,$$

(2.27)

$$(\boldsymbol{u}_{t}, \boldsymbol{v}) + (\nu(\Phi)D(\boldsymbol{u}), D(\boldsymbol{v})) + ((\boldsymbol{u} \cdot \nabla)\boldsymbol{u}, \boldsymbol{v}) - (p, \nabla \cdot \boldsymbol{v}) + (\Phi\nabla W, \boldsymbol{v})$$

$$= -\mu((\boldsymbol{v} \cdot \nabla)\boldsymbol{m}, \nabla\varphi) - \mu((\nabla \cdot \boldsymbol{v})\boldsymbol{m}, \nabla\varphi) + \frac{\mu}{2}(\boldsymbol{m} \times \nabla\varphi, \nabla \times \boldsymbol{v}),$$

(2.28)

$$(\nabla \cdot \boldsymbol{u}, q) = 0,$$

(2.29)

$$(\nabla \varphi_t, \nabla \psi) + \frac{1}{\tau} (\nabla \varphi, \nabla \psi) + \frac{1}{\tau} (\chi(\Phi) \nabla \varphi, \nabla \psi) + \beta (\boldsymbol{m} \times \nabla \varphi, \boldsymbol{m} \times \nabla \psi) - ((\boldsymbol{u} \cdot \nabla) \boldsymbol{m}, \nabla \psi) + \frac{1}{2} (\nabla \times \boldsymbol{u} \times \boldsymbol{m}, \nabla \psi) = \frac{1}{\tau} (\boldsymbol{h}_a, \nabla \psi) + (\boldsymbol{h}_b, \nabla \psi),$$

(2.30)

$$(\boldsymbol{m}_t, \boldsymbol{n}) + ((\boldsymbol{u} \cdot \nabla)\boldsymbol{m}, \boldsymbol{n}) - \frac{1}{2}(\nabla \times \boldsymbol{u} \times \boldsymbol{m}, \boldsymbol{n}) - \beta(\boldsymbol{m} \times \boldsymbol{h}, \boldsymbol{m} \times \boldsymbol{n}) + \frac{1}{\tau}(\boldsymbol{m}, \boldsymbol{n})$$

= $\frac{1}{\tau}(\chi(\Phi)\boldsymbol{h}, \boldsymbol{n})$.

2.3. The augmented system using the "zero-energy-contribution" feature. It can be seen that the (2.24)–(2.30) form a highly coupled system. In order to develop an easy-to-implement numerical algorithm, the key issue is to process the nonlinear coupling terms to obtain the desired decoupling type scheme, while obtaining second-order accuracy in time and maintaining energy stability unconditionally. To this end, we will exploit an obvious and therefore easily overlooked feature, the so-called zero-energy-contribution property that is satisfied by many nonlinear coupling terms. Details are shown below.

By setting $\Lambda = W$ in (2.24), $\boldsymbol{v} = \boldsymbol{u}$ in (2.27), $\psi = \mu \varphi$ in (2.29), and $\boldsymbol{n} = \frac{\mu}{\chi_0} \boldsymbol{m}$ in (2.30), using $\nabla \cdot \boldsymbol{u} = 0$, $\boldsymbol{u}|_{\partial\Omega} = \boldsymbol{0}$, $\boldsymbol{m} \times \boldsymbol{m} = \boldsymbol{0}$, and integration by parts, the following five equalities hold:

$$(2.31) \begin{cases} -(\boldsymbol{u}\Phi,\nabla W) + (\Phi\nabla W,\boldsymbol{u}) = 0, \\ ((\boldsymbol{u}\cdot\nabla)\boldsymbol{u},\boldsymbol{u}) = 0, \\ \mu((\boldsymbol{u}\cdot\nabla)\boldsymbol{m},\nabla\varphi) + \mu((\nabla\cdot\boldsymbol{u})\boldsymbol{m},\nabla\varphi) - \mu((\boldsymbol{u}\cdot\nabla)\boldsymbol{m},\nabla\varphi) = 0, \\ -\frac{\mu}{2}(\boldsymbol{m}\times\nabla\varphi,\nabla\times\boldsymbol{u}) + \frac{\mu}{2}(\nabla\times\boldsymbol{u}\times\boldsymbol{m},\nabla\varphi) = 0, \\ \frac{\mu}{\chi_0}((\boldsymbol{u}\cdot\nabla)\boldsymbol{m},\boldsymbol{m}) - \frac{\mu}{\chi_0}\frac{1}{2}(\nabla\times\boldsymbol{u}\times\boldsymbol{m},\boldsymbol{m}) - \frac{\mu}{\chi_0}\beta(\boldsymbol{m}\times\boldsymbol{h},\boldsymbol{m}\times\boldsymbol{m}) = 0. \end{cases}$$

These equations imply that the inner products formed by these nonlinear coupling terms and some special test functions are all zero. And these test functions are those special functions that must be used to obtain the total energy of the system. In other words, the contributions of these coupling terms to the total energy actually add up to zero; i.e., they satisfy the so-called zero-energy-contribution characteristic.

Inspired by [54, 55], which consider simpler phase-field type models coupled with hydrodynamics, e.g., no magnetic field case, we define a nonlocal auxiliary variable Q(t) and its associated ODE system as

$$\begin{cases}
Q_{t} = ((\boldsymbol{u} \cdot \nabla)\boldsymbol{u}, \boldsymbol{u}) - (\boldsymbol{u}\Phi, \nabla W) + (\Phi\nabla W, \boldsymbol{u}) + \mu((\boldsymbol{u} \cdot \nabla)\boldsymbol{m}, \nabla\varphi) \\
+ \mu((\nabla \cdot \boldsymbol{u})\boldsymbol{m}, \nabla\varphi) - \mu((\boldsymbol{u} \cdot \nabla)\boldsymbol{m}, \nabla\varphi) \\
- \frac{\mu}{2}(\boldsymbol{m} \times \nabla\varphi, \nabla \times \boldsymbol{u}) + \frac{\mu}{2}(\nabla \times \boldsymbol{u} \times \boldsymbol{m}, \nabla\varphi) \\
+ \frac{\mu}{\chi_{0}}((\boldsymbol{u} \cdot \nabla)\boldsymbol{m}, \boldsymbol{m}) - \frac{\mu}{\chi_{0}} \frac{1}{2}(\nabla \times \boldsymbol{u}, \boldsymbol{m} \times \boldsymbol{m}) - \frac{\mu}{\chi_{0}} \beta(\boldsymbol{m} \times \boldsymbol{h}, \boldsymbol{m} \times \boldsymbol{m}), \\
Q|_{t=0} = 1.
\end{cases}$$

Using the five equalities in (2.31) and the initial data, we find $Q_t = 0$ and $Q|_{t=0} = 1$. The ODE (2.32) actually defines a trivial solution of $Q(t) \equiv 1$.

Then, by multiplying the Q to those nonlinear terms contained in (2.32) (note: those terms will not change since $Q(t) \equiv 1$), we obtain an augmented equivalent system: find $(\Phi, W) \in H^1(\Omega)^2$, $\mathbf{u} \in \mathbf{H}_0^1(\Omega)$, $p \in L_0^2(\Omega)$, $\varphi \in H^1(\Omega) \cap L_0^2(\Omega)$, $\mathbf{m} \in \mathbf{H}^1(\Omega)$, such that for all $(\Lambda, X) \in H^1(\Omega)^2$, $\mathbf{v} \in \mathbf{H}_0^1(\Omega)$, $q \in L_0^2(\Omega)$, $\psi \in H^1(\Omega) \cap L_0^2(\Omega)$, $\mathbf{n} \in \mathbf{H}^1(\Omega)$, the following hold:

$$(2.33)$$

$$(\Phi_{t}, \Lambda) - Q(\boldsymbol{u}\Phi, \nabla\Lambda) = -M(\nabla W, \nabla\Lambda),$$

$$(2.34)$$

$$(W, X) = \lambda \epsilon(\nabla \Phi, \nabla X) + \lambda(H(\Phi)U, X) + \frac{S\lambda}{\epsilon}(\Phi, X),$$

$$(2.35)$$

$$U_{t} = \frac{1}{2}H(\Phi)\Phi_{t},$$

$$(2.36)$$

$$(\boldsymbol{u}_{t}, \boldsymbol{v}) + (\nu(\Phi)D(\boldsymbol{u}), D(\boldsymbol{v})) + Q((\boldsymbol{u} \cdot \nabla)\boldsymbol{u}, \boldsymbol{v}) - (p, \nabla \cdot \boldsymbol{v}) + Q(\Phi\nabla W, \boldsymbol{v})$$

$$= -Q\mu((\boldsymbol{v} \cdot \nabla)\boldsymbol{m}, \nabla\varphi) - Q\mu((\nabla \cdot \boldsymbol{v})\boldsymbol{m}, \nabla\varphi) + Q\frac{\mu}{2}(\boldsymbol{m} \times \nabla\varphi, \nabla \times \boldsymbol{v}),$$

$$(2.37)$$

$$(\nabla \cdot \boldsymbol{u}, q) = 0,$$

$$(2.38)$$

$$(\nabla\varphi_{t}, \nabla\psi) + \frac{1}{\tau}(\nabla\varphi, \nabla\psi) + \frac{1}{\tau}(\chi(\Phi)\nabla\varphi, \nabla\psi) - Q((\boldsymbol{u} \cdot \nabla)\boldsymbol{m}, \nabla\psi)$$

$$+Q\frac{1}{2}(\nabla \times \boldsymbol{u} \times \boldsymbol{m}, \nabla \psi) + \beta(\boldsymbol{m} \times \nabla \varphi, \boldsymbol{m} \times \nabla \psi) = \frac{1}{\tau}(\boldsymbol{h}_{a}, \nabla \psi) + (\boldsymbol{h}_{b}, \nabla \psi),$$

$$(2.39)$$

$$(\boldsymbol{m}_{t}, \boldsymbol{n}) + Q((\boldsymbol{u} \cdot \nabla)\boldsymbol{m}, \boldsymbol{n}) - Q\frac{1}{2}(\nabla \times \boldsymbol{u} \times \boldsymbol{m}, \boldsymbol{n}) - Q\beta(\boldsymbol{m} \times \boldsymbol{h}, \boldsymbol{m} \times \boldsymbol{n}) + \frac{1}{\tau}(\boldsymbol{m}, \boldsymbol{n})$$

$$= \frac{1}{\tau}(\chi(\Phi)\boldsymbol{h}, \boldsymbol{n}),$$

$$(2.40)$$

$$Q_{t} = ((\boldsymbol{u} \cdot \nabla)\boldsymbol{u}, \boldsymbol{u}) - (\boldsymbol{u}\Phi, \nabla W) + (\Phi\nabla W, \boldsymbol{u})$$

$$+ \mu((\boldsymbol{u} \cdot \nabla)\boldsymbol{m}, \nabla \varphi) + \mu((\nabla \cdot \boldsymbol{u})\boldsymbol{m}, \nabla \varphi) - \mu((\boldsymbol{u} \cdot \nabla)\boldsymbol{m}, \nabla \varphi)$$

$$- \frac{\mu}{2}(\boldsymbol{m} \times \nabla \varphi, \nabla \times \boldsymbol{u}) + \frac{\mu}{2}(\nabla \times \boldsymbol{u} \times \boldsymbol{m}, \nabla \varphi)$$

$$+ \frac{\mu}{\chi_{0}}((\boldsymbol{u} \cdot \nabla)\boldsymbol{m}, \boldsymbol{m}) - \frac{\mu}{\chi_{0}}\frac{1}{2}(\nabla \times \boldsymbol{u}, \boldsymbol{m} \times \boldsymbol{m}) - \frac{\mu}{\chi_{0}}\beta(\boldsymbol{m} \times \boldsymbol{h}, \boldsymbol{m} \times \boldsymbol{m}),$$

$$(2.41)$$

$$Q_{t=0} = 1.$$

Remark 2.3. Note that although the system (2.33)–(2.41) seems to be more complex than the original model (2.3)–(2.10), it is an "algorithm-friendly" form. That is, we will eventually find that the new system obtained after reformulation has at least two advantages for numerical discretization: (i) the discretization of many nonlinear terms in the new system will be very simple and convenient, and hence we no longer need to determine which terms are implicit or explicit (since every term with the "zero-energy-contribution" feature can be simply discretized explicitly); (ii) the numerical implementation of the final scheme will be very simple; that is, we only need to solve a few independent decoupled elliptic equations at each time step, without adding any computational complexity to the algorithm at all. It is worth spending two intermediate steps (in sections 2.2 and 2.3) to reconstruct the original system at the PDE level, making it relatively easy to obtain an effective numerical algorithm for such a complex model, in which the computational cost can be reduced in practical numerical implementation.

In the following theorem, we show that the newly reformulated system (2.33)–(2.41) admits the energy estimate.

Theorem 2.1. Assuming $\chi(\Phi) \leq \chi_0$, the system (2.33)–(2.41) satisfies the energy stability

(2.42)
$$\frac{d}{dt}E_{mod}(\Phi, U, \boldsymbol{u}, \boldsymbol{h}, \boldsymbol{m}, Q) + D(W, \boldsymbol{u}, \boldsymbol{h}, \boldsymbol{m}) \leq \frac{\mu}{\tau} \|\boldsymbol{h}_a\|^2 + \tau \mu \|\boldsymbol{h}_b\|^2.$$

For the case of no applied magnetic field ($h_a = 0$), the following energy dissipation law holds:

(2.43)
$$\frac{d}{dt}E_{mod}(\Phi, U, \boldsymbol{u}, \boldsymbol{h}, \boldsymbol{m}, Q) + D(W, \boldsymbol{u}, \boldsymbol{h}, \boldsymbol{m}) \leq 0.$$

Here

(2.44)
$$E_{mod}(\Phi, U, \boldsymbol{u}, \boldsymbol{h}, \boldsymbol{m}, Q) = \lambda \left(\frac{\epsilon}{2} \|\nabla \Phi\|^2 + \frac{S}{2\epsilon} \|\Phi\|^2 + \|U\|^2 \right) + \frac{1}{2} \|\boldsymbol{u}\|^2 + \frac{\mu}{2} \|\boldsymbol{h}\|^2 + \frac{\mu}{2\chi_0} \|\boldsymbol{m}\|^2 + \frac{1}{2} |Q|^2 - \lambda B|\Omega| - \frac{1}{2}.$$

Proof. By setting $\Lambda = W$ in (2.33), $X = \Phi_t$ in (2.34), and taking the L^2 inner product of (2.35) with $2\lambda U$, we get

$$\begin{split} &(\Phi_t, W) - Q(\boldsymbol{u}\Phi, \nabla W) + M\|\nabla W\|^2 = 0, \\ &(W, \Phi_t) = \frac{\lambda \epsilon}{2} \frac{d}{dt} \|\nabla \Phi\|^2 + \lambda (H(\Phi)U, \Phi_t) + \frac{S\lambda}{2\epsilon} \frac{d}{dt} \|\Phi\|^2, \quad \lambda \frac{d}{dt} \|U\|^2 = \lambda (H(\Phi)\Phi_t, U). \end{split}$$

We combine the above obtained equations to get

$$(2.45) \quad \frac{\lambda \epsilon}{2} \frac{d}{dt} \|\nabla \Phi\|^2 + \frac{S\lambda}{2\epsilon} \frac{d}{dt} \|\Phi\|^2 + \lambda \frac{d}{dt} \|U\|^2 - Q(\boldsymbol{u}\Phi, \nabla W) + M \|\nabla W\|^2 = 0.$$

By taking $\mathbf{v} = \mathbf{u}$ in (2.36), q = p in (2.37), we derive

(2.46)

$$\frac{1}{2} \frac{d}{dt} \|\mathbf{u}\|^{2} + \|\sqrt{\nu(\Phi)}D(\mathbf{u})\|^{2} + Q((\mathbf{u} \cdot \nabla)\mathbf{u}, \mathbf{u}) + Q(\Phi\nabla W, \mathbf{u})$$

$$= -Q\mu((\mathbf{u} \cdot \nabla)\mathbf{m}, \nabla\varphi) - Q\mu((\nabla \cdot \mathbf{u})\mathbf{m}, \nabla\varphi) + Q\frac{\mu}{2}(\mathbf{m} \times \nabla\varphi, \nabla \times \mathbf{u}).$$

By taking $\psi = \mu \varphi$ in (2.38), and noting that $\mathbf{h} = \nabla \varphi$, we have

(2.47)

$$\frac{\mu}{2} \frac{d}{dt} \|\mathbf{h}\|^2 + \frac{\mu}{\tau} \|\mathbf{h}\|^2 + \frac{\mu}{\tau} \|\sqrt{\chi(\Phi)}\mathbf{h}\|^2 - Q\mu((\mathbf{u} \cdot \nabla)\mathbf{m}, \nabla\varphi) + Q\frac{\mu}{2} (\nabla \times \mathbf{u} \times \mathbf{m}, \nabla\varphi) + \beta\mu \|\mathbf{m} \times \mathbf{h}\|^2 = \mu(\mathbf{h}_b, \mathbf{h}) + \frac{\mu}{\tau} (\mathbf{h}_a, \mathbf{h}).$$

By taking $\boldsymbol{n} = \frac{\mu}{\chi_0} \boldsymbol{m}$ in (2.39), we get

(2.48)

$$\begin{split} \frac{1}{2} \frac{\mu}{\chi_0} \frac{d}{dt} \| \boldsymbol{m} \|^2 + Q \frac{\mu}{\chi_0} ((\boldsymbol{u} \cdot \nabla) \boldsymbol{m}, \boldsymbol{m}) - Q \frac{\mu}{\chi_0} \frac{1}{2} (\nabla \times \boldsymbol{u}, \boldsymbol{m} \times \boldsymbol{m}) \\ - Q \frac{\mu}{\chi_0} \beta (\boldsymbol{m} \times \boldsymbol{h}, \boldsymbol{m} \times \boldsymbol{m}) \\ + \frac{\mu}{\chi_0} \frac{1}{\tau} \| \boldsymbol{m} \|^2 &= \frac{\mu}{\chi_0} \frac{1}{\tau} (\chi(\Phi) \boldsymbol{h}, \boldsymbol{m}). \end{split}$$

By multiplying Q for both sides of (2.40), we obtain

(2.49)

$$\begin{split} \frac{1}{2}\frac{d}{dt}|Q|^2 &= Q((\boldsymbol{u}\cdot\nabla)\boldsymbol{u},\boldsymbol{u}) - Q(\boldsymbol{u}\Phi,\nabla W) + Q(\Phi\nabla W,\boldsymbol{u}) + \mu Q((\boldsymbol{u}\cdot\nabla)\boldsymbol{m},\nabla\varphi) \\ &+ \mu Q((\nabla\cdot\boldsymbol{u})\boldsymbol{m},\nabla\varphi) - \mu Q((\boldsymbol{u}\cdot\nabla)\boldsymbol{m},\nabla\varphi) \\ &- \frac{\mu}{2}Q(\boldsymbol{m}\times\nabla\varphi,\nabla\times\boldsymbol{u}) + \frac{\mu}{2}Q(\nabla\times\boldsymbol{u}\times\boldsymbol{m},\nabla\varphi) \\ &+ \frac{\mu}{\chi_0}Q((\boldsymbol{u}\cdot\nabla)\boldsymbol{m},\boldsymbol{m}) - \frac{\mu}{\chi_0}\frac{1}{2}Q(\nabla\times\boldsymbol{u},\boldsymbol{m}\times\boldsymbol{m}) - \frac{\mu}{\chi_0}\beta Q(\boldsymbol{m}\times\boldsymbol{h},\boldsymbol{m}\times\boldsymbol{m}). \end{split}$$

By combining (2.45)–(2.49), we arrive at

(2.50)

$$\frac{d}{dt} \left(\frac{\lambda \epsilon}{2} \|\nabla \Phi\|^2 + \frac{S\lambda}{2\epsilon} \|\Phi\|^2 + \lambda \|U\|^2 + \frac{1}{2} \|\boldsymbol{u}\|^2 + \frac{\mu}{2} \|\boldsymbol{h}\|^2 + \frac{\mu}{2\chi_0} \|\boldsymbol{m}\|^2 + \frac{1}{2} |Q|^2 \right)
+ M \|\nabla W\|^2 + \left\| \sqrt{\nu(\Phi)} D(\boldsymbol{u}) \right\|^2 + \frac{\mu}{\tau} \|\boldsymbol{h}\|^2 + \frac{\mu}{\tau} \|\sqrt{\chi(\Phi)} \boldsymbol{h} \|^2
+ \beta \mu \|\boldsymbol{m} \times \boldsymbol{h}\|^2 + \frac{\mu}{\tau\chi_0} \|\boldsymbol{m}\|^2
= \frac{\mu}{\tau} (\boldsymbol{h}_a, \boldsymbol{h}) + \mu (\boldsymbol{h}_b, \boldsymbol{h}) + \frac{\mu}{\tau\chi_0} (\chi(\Phi) \boldsymbol{h}, \boldsymbol{m}).$$

Moreover, by applying the Cauchy-Schwarz inequality, we derive

(2.51)

$$\frac{\mu}{\tau \chi_0} (\chi(\Phi) \boldsymbol{h}, \boldsymbol{m}) \leq \frac{\mu}{\tau \chi_0} \left\| \sqrt{\chi(\Phi)} \boldsymbol{h} \right\| \left\| \sqrt{\chi(\Phi)} \boldsymbol{m} \right\| \leq \frac{\mu}{\tau} \left\| \sqrt{\chi(\Phi)} \boldsymbol{h} \right\|^2 + \frac{\mu}{4\tau \chi_0^2} \left\| \sqrt{\chi(\Phi)} \boldsymbol{m} \right\|^2$$
$$\leq \frac{\mu}{\tau} \left\| \sqrt{\chi(\Phi)} \boldsymbol{h} \right\|^2 + \frac{\mu}{4\tau \chi_0^2} \chi_0 \| \boldsymbol{m} \|^2$$

and

(2.52)
$$\frac{\mu}{\tau}(\boldsymbol{h}_a, \boldsymbol{h}) + \mu(\boldsymbol{h}_b, \boldsymbol{h}) \leq \frac{\mu}{\tau} \|\boldsymbol{h}_a\| \|\boldsymbol{h}\| + \mu \|\boldsymbol{h}_b\| \|\boldsymbol{h}\|$$
$$\leq \frac{\mu}{4\tau} \|\boldsymbol{h}\|^2 + \frac{\mu}{\tau} \|\boldsymbol{h}_a\|^2 + \frac{\mu}{4\tau} \|\boldsymbol{h}\|^2 + \tau \mu \|\boldsymbol{h}_b\|^2.$$

Finally, by combining (2.50), (2.51), and (2.52), we obtain

$$\begin{split} \frac{d}{dt} \left(\frac{\lambda \epsilon}{2} \| \nabla \Phi \|^2 + \frac{S\lambda}{2\epsilon} \| \Phi \|^2 + \lambda \| U \|^2 + \frac{1}{2} \| \boldsymbol{u} \|^2 + \frac{\mu}{2} \| \boldsymbol{h} \|^2 + \frac{\mu}{2\chi_0} \| \boldsymbol{m} \|^2 + \frac{1}{2} |Q|^2 \right) \\ + M \| \nabla W \|^2 + \left\| \sqrt{\nu(\Phi)} D(\boldsymbol{u}) \right\|^2 + \frac{\mu}{2\tau} \| \boldsymbol{h} \|^2 + \beta \mu \| \boldsymbol{m} \times \boldsymbol{h} \|^2 + \frac{3\mu}{4\tau\chi_0} \| \boldsymbol{m} \|^2 \\ \leq \frac{\mu}{\tau} \| \boldsymbol{h}_a \|^2 + \tau \mu \| \boldsymbol{h}_b \|^2, \end{split}$$

which completes the proof.

Remark 2.4. First, we explain why an adjustable quadratic term $\frac{S}{2\epsilon}\Phi^2$ is extracted from the nonlinear term $F(\Phi)$ when we define the new variable U. From the form of the original energy $E(\Phi, \boldsymbol{u}, \boldsymbol{h}, \boldsymbol{m})$ given in (2.11), we find that H^1 -stability Φ is guaranteed since the L^2 -norm of Φ is always bounded by the L^4 -norm, which is contained in the term $F(\Phi)$. Thus, when designing the numerical scheme, to guarantee the H^1 -stability of the numerical solution, we extract the quadratic term $\frac{S}{2\epsilon}\Phi^2$ from the nonlinear potential $F(\Phi)$. In this way, this term, together with the gradient potential of $\|\nabla \Phi\|^2$, can guarantee the H^1 -stability of Φ in the modified energy. Since the special feature of the IEQ method is that the nonlinear term $F(\Phi)$ is replaced by the new variable U, this form of replacement will result in the loss of the L^2 -norm of the variable Φ . That is, if S=0 in (2.44), then the H^1 -stability of Φ cannot be guaranteed, leading to instabilities in actual computations while using larger time steps.

Second, we explain how to set the magnitude of S in practice. Since the magnitude of the L^4 -norm of Φ from the original energy (2.11) is about $1/\epsilon$, and hence in the modified energy, the magnitude of the L^2 -norm caused by the stabilizer S should also be the same scale as the original L^4 -norm. That is, $S \sim O(1)$. Such a linear stabilization technique has been extensively used to construct numerical schemes for solving various nonlinear models, such as IEQ, SAV, convex splitting methods, etc.; cf. [8, 41, 42, 45].

Third, it is easy to see that the modified energy (2.44) is equivalent to the original energy (2.11) after we add two constants $-\lambda B|\Omega| - \frac{1}{2}$ in (2.44).

3. Numerical scheme. So far, we have made sufficient preparations for the construction of the linear, second-order, fully decoupled, unconditionally energy stable, continuous finite element scheme for the two-phase FHD system (2.3)–(2.10).

3.1. Fully discrete scheme. Assume that the polygonal/polyhedral domain Ω is discretized by a conforming and shape regular triangulation/tetrahedron mesh \mathcal{T}_h that is composed by open disjoint elements K such that $\bar{\Omega} = \bigcup_{K \in \mathcal{T}_h} \bar{K}$. We use \mathcal{P}_l to denote the space of polynomials of total degree at most l. We introduce several conforming finite element spaces as follows:

$$Y_{h} = \left\{ X \in H^{1}(\Omega) : X|_{K} \in \mathcal{P}_{l_{1}}(K) \,\forall K \in \mathcal{T}_{h} \right\},$$

$$\mathbf{V}_{h} = \left\{ \mathbf{v} \in \mathbf{H}_{0}^{1}(\Omega) : \mathbf{v}|_{K} \in \mathcal{P}_{l_{2}}(K)^{d} \,\forall K \in \mathcal{T}_{h} \right\},$$

$$Q_{h} = \left\{ q \in H^{1}(\Omega) \cap L_{0}^{2}(\Omega) : q|_{K} \in \mathcal{P}_{l_{2}-1}(K) \,\forall K \in \mathcal{T}_{h} \right\},$$

$$\Psi_{h} = \left\{ \psi \in H^{1}(\Omega) \cap L_{0}^{2}(\Omega) : \psi|_{K} \in \mathcal{P}_{l_{3}}(K) \,\forall K \in \mathcal{T}_{h} \right\},$$

$$\mathbf{N}_{h} = \left\{ \mathbf{n} \in \mathbf{H}^{1}(\Omega) : \mathbf{n}|_{K} \in \mathcal{P}_{l_{3}-1}(K)^{d} \,\forall K \in \mathcal{T}_{h} \right\}.$$

We assume the pair of spaces (V_h, Q_h) satisfy the *inf-sup* condition [16]: $\beta_0 ||q|| \le \sup_{\boldsymbol{v} \in \boldsymbol{V}_h} \frac{(\nabla \cdot \boldsymbol{v}, q)}{||\nabla \boldsymbol{v}||}$ for all $q \in Q_h$, where the constant β_0 only depends on Ω . Some *inf-sup* stable pairs (\boldsymbol{V}_h, Q_h) are known in [16].

Let N>0 denote the total number of time steps, define the uniform time step size as $\delta t = [\frac{T}{N}]$, and set $t_n = n\delta t$. For convenience, we define the first-order temporal discretization operator as $d_t w^{n+1} = \frac{w^{n+1}-w^n}{\delta t}$, the second-order temporal discretization operator as $D_t w^{n+1} = \frac{3w^{n+1}-4w^n+w^{n-1}}{2\delta t}$, and the second-order explicit extrapolation operator as $w^* = 2w^n - w^{n-1}$ for any variable w.

Then the fully discrete numerical scheme for (2.33)–(2.41) reads as follows: find $(\Phi^{n+1}, W^{n+1}) \in Y_h^2$, $\tilde{\boldsymbol{u}}^{n+1} \in \boldsymbol{V}_h$, $p^{n+1} \in Q_h$, $\boldsymbol{u}^{n+1} \in \boldsymbol{V}_h + \nabla Q_h$, $\varphi^{n+1} \in \Psi_h$, $\boldsymbol{m}^{n+1} \in \boldsymbol{N}_h$, and $Q^{n+1} \in R$ such that

$$(\frac{a\Phi^{n+1} - b\Phi^n + c\Phi^{n-1}}{2\delta t}, \Lambda) - Q^{n+1}(\boldsymbol{u}^*\Phi^*, \nabla\Lambda) + M(\nabla W^{n+1}, \nabla\Lambda) = 0,$$

$$(3.3)$$

$$(W^{n+1}, X) = \lambda \epsilon (\nabla \Phi^{n+1}, \nabla X) + \lambda (H(\Phi^*)U^{n+1}, X) + \frac{S\lambda}{\epsilon} (\Phi^{n+1}, X),$$

$$3.4)$$

$$aU^{n+1} - bU^n + cU^{n-1} = \frac{1}{2}H(\Phi^*)(a\Phi^{n+1} - b\Phi^n + c\Phi^{n-1}),$$

$$(3.5)$$

$$\left(\frac{a\tilde{\boldsymbol{u}}^{n+1} - b\boldsymbol{u}^n + c\boldsymbol{u}^{n-1}}{2\delta t}, \boldsymbol{v}\right) + (\nu(\Phi^*)D(\tilde{\boldsymbol{u}}^{n+1}), D(\boldsymbol{v})) + (\nabla p^n, \boldsymbol{v})$$

$$+ Q^{n+1}((\boldsymbol{u}^* \cdot \nabla)\boldsymbol{u}^*, \boldsymbol{v}) + Q^{n+1}(\Phi^*\nabla W^*, \boldsymbol{v})$$

$$= -Q^{n+1}\mu((\boldsymbol{v} \cdot \nabla)\boldsymbol{m}^*, \nabla \varphi^*) - Q^{n+1}\mu((\nabla \cdot \boldsymbol{v})\boldsymbol{m}^*, \nabla \varphi^*)$$

$$+ Q^{n+1}\frac{\mu}{2}(\boldsymbol{m}^* \times \nabla \varphi^*, \nabla \times \boldsymbol{v}),$$

$$(3.6)$$

$$(\nabla p^{n+1}, \nabla q) = -\frac{a}{2\delta t}(\nabla \cdot \tilde{\boldsymbol{u}}^{n+1}, q) + (\nabla p^n, \nabla q),$$

$$(3.7)$$

$$\boldsymbol{u}^{n+1} = \tilde{\boldsymbol{u}}^{n+1} - \frac{2\delta t}{a}\nabla p^{n+1} + \frac{2\delta t}{a}\nabla p^n,$$

$$(3.8)$$

$$\left(\frac{a\nabla \varphi^{n+1} - b\nabla \varphi^n + c\nabla \varphi^{n-1}}{2\delta t}, \nabla \psi\right) + \frac{1}{\tau}(\nabla \varphi^{n+1}, \nabla \psi) + \frac{1}{\tau}(\chi(\Phi^*)\nabla \varphi^{n+1}, \nabla \psi)$$

$$\begin{split} &-Q^{n+1}((\boldsymbol{u}^*\cdot\nabla)\boldsymbol{m}^*,\nabla\psi)+Q^{n+1}\frac{1}{2}(\nabla\times\boldsymbol{u}^*\times\boldsymbol{m}^*,\nabla\psi)\\ &+\beta(\boldsymbol{m}^*\times\nabla\varphi^{n+1},\boldsymbol{m}^*\times\nabla\psi)\\ &=(\boldsymbol{h}_b^{n+1},\nabla\psi)+\frac{1}{\tau}(\boldsymbol{h}_a^{n+1},\nabla\psi),\\ (3.9)\\ &\left(\frac{a\boldsymbol{m}^{n+1}-b\boldsymbol{m}^n+c\boldsymbol{m}^{n-1}}{2\delta t},\boldsymbol{n}\right)+Q^{n+1}((\boldsymbol{u}^*\cdot\nabla)\boldsymbol{m}^*,\boldsymbol{n})-Q^{n+1}\frac{1}{2}(\nabla\times\boldsymbol{u}^*\times\boldsymbol{m}^*,\boldsymbol{n})\\ &-Q^{n+1}\beta(\boldsymbol{m}^*\times\boldsymbol{h}^*,\boldsymbol{m}^*\times\boldsymbol{n})+\frac{1}{\tau}(\boldsymbol{m}^{n+1},\boldsymbol{n})=\frac{1}{\tau}(\chi(\Phi^*)\boldsymbol{h}^{n+1},\boldsymbol{n}),\\ (3.10)\\ &\frac{aQ^{n+1}-bQ^n+cQ^{n-1}}{2\delta t}=((\boldsymbol{u}^*\cdot\nabla)\boldsymbol{u}^*,\tilde{\boldsymbol{u}}^{n+1})-(\boldsymbol{u}^*\Phi^*,\nabla W^{n+1})+(\Phi^*\nabla W^*,\tilde{\boldsymbol{u}}^{n+1})\\ &+\mu((\tilde{\boldsymbol{u}}^{n+1}\cdot\nabla)\boldsymbol{m}^*,\nabla\varphi^*)+\mu((\nabla\cdot\tilde{\boldsymbol{u}}^{n+1})\boldsymbol{m}^*,\nabla\varphi^*)-\mu((\boldsymbol{u}^*\cdot\nabla)\boldsymbol{m}^*,\nabla\varphi^{n+1})\\ &-\frac{\mu}{2}(\boldsymbol{m}^*\times\nabla\varphi^*,\nabla\times\tilde{\boldsymbol{u}}^{n+1})+\frac{\mu}{2}(\nabla\times\boldsymbol{u}^*\times\boldsymbol{m}^*,\nabla\varphi^{n+1})\\ &+\frac{\mu}{\chi_0}((\boldsymbol{u}^*\cdot\nabla)\boldsymbol{m}^*,\boldsymbol{m}^{n+1})-\frac{\mu}{\chi_0}\frac{1}{2}(\nabla\times\boldsymbol{u}^*,\boldsymbol{m}^*\times\boldsymbol{m}^{n+1})\\ &-\frac{\mu}{\gamma_0}\beta(\boldsymbol{m}^*\times\boldsymbol{h}^*,\boldsymbol{m}^*\times\boldsymbol{m}^{n+1})\end{split}$$

for all $(\Lambda, X) \in Y_h^2$, $\boldsymbol{v} \in \boldsymbol{V}_h$, $q \in Q_h$, $\psi \in \Psi_h$, and $\boldsymbol{n} \in \boldsymbol{N}_h$, where a = 3, b = 4, c = 1, and $\boldsymbol{h}^n = \nabla \varphi^n$. Several remarks are in order to explain the details of the above scheme.

Remark 3.1. We use the second-order pressure projection method [18, 39] to decouple the linear coupling between the velocity field \boldsymbol{u} and the pressure p in the fluid momentum equation. All temporal derivatives are discretized using the second-order backward differential formula (BDF2). All nonlinear coupling terms that satisfy the "zero-energy-contribution" characteristic are discretized explicitly, while the multiplier Q of these terms is implicitly discretized. The positive definite nonlinear term $\beta(\boldsymbol{m} \times \nabla \varphi, \boldsymbol{m} \times \nabla \psi)$ is handled by an appropriate two-step implicit-explicit format.

Remark 3.2. From (3.4), one can rewrite U^{n+1} as follows:

$$(3.11) \quad U^{n+1} = \frac{1}{2}H(\Phi^*)\Phi^{n+1} - \frac{2}{3}H(\Phi^*)\Phi^n + \frac{1}{6}H(\Phi^*)\Phi^{n-1} + \frac{4}{3}U^n - \frac{1}{3}U^{n-1}.$$

The above form (3.11) can be substituted into (3.3). In this way, once Φ^{n+1} is obtained, then U^{n+1} will be updated by (3.11) later.

Remark 3.3. The marching of the scheme (3.2)–(3.10) needs the solution of the first time step $t = \delta t$, which can be easily obtained from the first-order scheme by setting a = 2, b = 2, c = 0, and $w^* = w^n$ for $w = \Phi$, u, W, φ , and m in (3.2)–(3.10).

Remark 3.4. It can be verified that the final velocity field u^{n+1} in the above scheme (3.2)–(3.10) satisfies the following weakly discrete divergence-free condition:

$$(3.12) (\boldsymbol{u}^{n+1}, \nabla q) = 0 \ \forall q \in Q_h.$$

In the following, we show that the scheme (3.2)–(3.10) holds the unconditional energy law.

THEOREM 3.1. Assuming $\chi(\Phi) \leq \chi_0$, the scheme (3.2)–(3.10) satisfies the following energy stability unconditionally:

$$d_t \widetilde{E}^{n+1} + \widetilde{D}^{n+1} \leq \frac{\mu}{\tau} \|\boldsymbol{h}_a^{n+1}\|^2 + \tau \mu \|\boldsymbol{h}_b^{n+1}\|^2;$$

if the applied magnetic field $\mathbf{h}_a = \mathbf{0}$, then the scheme (3.2)–(3.10) holds the following energy dissipation law unconditionally:

$$d_t \widetilde{E}^{n+1} + \widetilde{D}^{n+1} \le 0,$$

where

$$\widetilde{E}^{n+1} = \frac{\lambda \epsilon}{4} (\|\nabla \Phi^{n+1}\|^2 + \|2\nabla \Phi^{n+1} - \nabla \Phi^n\|^2) + \frac{S\lambda}{4\epsilon} (\|\Phi^{n+1}\|^2 + \|2\Phi^{n+1} - \Phi^n\|^2)$$

$$+ \frac{\lambda}{2} (\|U^{n+1}\|^2 + \|2U^{n+1} - U^n\|^2) + \frac{1}{4} (\|\boldsymbol{u}^{n+1}\|^2 + \|2\boldsymbol{u}^{n+1} - \boldsymbol{u}^n\|^2)$$

$$+ \frac{\mu}{4} (\|\boldsymbol{h}^{n+1}\|^2 + \|2\boldsymbol{h}^{n+1} - \boldsymbol{h}^n\|^2) + \frac{\mu}{4\chi_0} (\|\boldsymbol{m}^{n+1}\|^2 + \|2\boldsymbol{m}^{n+1} - \boldsymbol{m}^n\|^2)$$

$$+ \frac{1}{4} (\|Q^{n+1}\|^2 + |2Q^{n+1} - Q^n|^2) + \frac{\delta t^2}{3} \|\nabla p^{n+1}\|^2$$

and

$$\widetilde{D}^{n+1} = M \|\nabla W^{n+1}\|^2 + \left\| \sqrt{\nu(\Phi^*)} D(\widetilde{\boldsymbol{u}}^{n+1}) \right\|^2 + \frac{3\mu}{4\tau\chi_0} \|\boldsymbol{m}^{n+1}\|^2 + \frac{\mu}{2\tau} \|\boldsymbol{h}^{n+1}\|^2 + \mu\beta \|\boldsymbol{m}^* \times \boldsymbol{h}^{n+1}\|^2.$$

Proof. By taking $\Lambda = W^{n+1}$ in (3.2), $X = D_t \Phi^{n+1}$ in (3.3), and the L^2 inner product of (3.4) with $\frac{\lambda}{\delta t} U^{n+1}$, we derive

$$(3.14) (D_t \Phi^{n+1}, W^{n+1}) - Q^{n+1}(\boldsymbol{u}^* \Phi^*, \nabla W^{n+1}) + M \|\nabla W^{n+1}\|^2 = 0,$$

$$(3.15) (W^{n+1}, D_t \Phi^{n+1}) = \lambda \epsilon (\nabla \Phi^{n+1}, \nabla D_t \Phi^{n+1}) + \lambda (H(\Phi^*) U^{n+1}, D_t \Phi^{n+1})$$

$$+ \frac{S\lambda}{\epsilon} (\Phi^{n+1}, D_t \Phi^{n+1})$$

and

(3.16)

$$2\lambda(D_t U^{n+1}, U^{n+1}) = \lambda(H(\Phi^*)D_t \Phi^{n+1}, U^{n+1}).$$

Combining (3.14)–(3.16) together, we get

(3.17)

$$\begin{split} &\frac{\lambda\epsilon}{4\delta t}(\|\nabla\Phi^{n+1}\|^2 - \|\nabla\Phi^n\|^2 \\ &+ \|2\nabla\Phi^{n+1} - \nabla\Phi^n\|^2 - \|2\nabla\Phi^n - \nabla\Phi^{n-1}\|^2 + \|\nabla\Phi^{n+1} - \nabla\Phi^*\|^2) \\ &+ \frac{S\lambda}{4\delta t\epsilon}(\|\Phi^{n+1}\|^2 - \|\Phi^n\|^2 + \|2\Phi^{n+1} - \Phi^n\|^2 - \|2\Phi^n - \Phi^{n-1}\|^2 + \|\Phi^{n+1} - \Phi^*\|^2) \\ &+ \frac{\lambda}{2\delta t}(\|U^{n+1}\|^2 - \|U^n\|^2 + \|2U^{n+1} - U^n\|^2 - \|2U^n - U^{n-1}\|^2 + \|U^{n+1} - U^*\|^2) \\ &- Q^{n+1}(\boldsymbol{u}^*\Phi^*, \nabla W^{n+1}) + M\|\nabla W^{n+1}\|^2 = 0, \end{split}$$

where we use the following identity:

$$(3.18) 2(3a - 4b + c, a) = a^2 - b^2 + (2a - b)^2 - (2b - c)^2 + (a - 2b + c)^2.$$

Taking $\mathbf{v} = \tilde{\mathbf{u}}^{n+1}$ in (3.5), we get

(3.19)

$$\begin{split} &\frac{1}{2\delta t}(3\tilde{\boldsymbol{u}}^{n+1}-4\boldsymbol{u}^n+\boldsymbol{u}^{n-1},\tilde{\boldsymbol{u}}^{n+1})+\left\|\sqrt{\nu(\Phi^*)}D(\tilde{\boldsymbol{u}}^{n+1})\right\|^2+(\nabla p^n,\tilde{\boldsymbol{u}}^{n+1})\\ &+Q^{n+1}((\boldsymbol{u}^*\cdot\nabla)\boldsymbol{u}^*,\tilde{\boldsymbol{u}}^{n+1})+Q^{n+1}(\Phi^*\nabla W^*,\tilde{\boldsymbol{u}}^{n+1})+Q^{n+1}\mu((\tilde{\boldsymbol{u}}^{n+1}\cdot\nabla)\boldsymbol{m}^*,\nabla\varphi^*)\\ &+Q^{n+1}\mu((\nabla\cdot\tilde{\boldsymbol{u}}^{n+1})\boldsymbol{m}^*,\nabla\varphi^*)-Q^{n+1}\frac{\mu}{2}(\boldsymbol{m}^*\times\nabla\varphi^*,\nabla\times\tilde{\boldsymbol{u}}^{n+1})=0. \end{split}$$

Taking $\psi = \mu \varphi^{n+1}$ in (3.8), and noticing $\mathbf{h}^n = \nabla \varphi^n$, we get

$$(3.20)$$

$$\frac{\mu}{4\delta t}(\|\boldsymbol{h}^{n+1}\|^{2} - \|\boldsymbol{h}^{n}\|^{2} + \|2\boldsymbol{h}^{n+1} - \boldsymbol{h}^{n}\|^{2} - \|2\boldsymbol{h}^{n} - \boldsymbol{h}^{n-1}\|^{2} + \|\boldsymbol{h}^{n+1} - \boldsymbol{h}^{*}\|^{2})$$

$$+ \frac{\mu}{\tau}\|\boldsymbol{h}^{n+1}\|^{2} + \frac{\mu}{\tau}\|\sqrt{\chi(\Phi^{*})}\boldsymbol{h}^{n+1}\|^{2} - Q^{n+1}\mu((\boldsymbol{u}^{*}\cdot\nabla)\boldsymbol{m}^{*},\nabla\varphi^{n+1})$$

$$+ Q^{n+1}\frac{\mu}{2}(\nabla\times\boldsymbol{u}^{*}\times\boldsymbol{m}^{*},\nabla\varphi^{n+1}) + \mu\beta\|\boldsymbol{m}^{*}\times\boldsymbol{h}^{n+1}\|^{2}$$

$$= \mu(\boldsymbol{h}_{b}^{n+1},\boldsymbol{h}^{n+1}) + \frac{\mu}{\tau}(\boldsymbol{h}_{a}^{n+1},\boldsymbol{h}^{n+1}).$$

Taking $\boldsymbol{n} = \frac{\mu}{\chi_0} \boldsymbol{m}^{n+1}$ in (3.9), we have

$$\frac{1}{4\delta t} \frac{\mu}{\chi_0} (\|\boldsymbol{m}^{n+1}\|^2 - \|\boldsymbol{m}^n\|^2 + \|2\boldsymbol{m}^{n+1} - \boldsymbol{m}^n\|^2 - \|2\boldsymbol{m}^n - \boldsymbol{m}^{n-1}\|^2 + \|\boldsymbol{m}^{n+1} - \boldsymbol{m}^*\|^2) \\
+ \frac{\mu}{\chi_0} \frac{1}{\tau} \|\boldsymbol{m}^{n+1}\|^2 + Q^{n+1} \frac{\mu}{\chi_0} ((\boldsymbol{u}^* \cdot \nabla) \boldsymbol{m}^*, \boldsymbol{m}^{n+1}) \\
- Q^{n+1} \frac{\mu}{\chi_0} \frac{1}{2} (\nabla \times \boldsymbol{u}^* \times \boldsymbol{m}^*, \boldsymbol{m}^{n+1}) \\
- Q^{n+1} \frac{\mu}{\chi_0} \beta(\boldsymbol{m}^* \times \boldsymbol{h}^*, \boldsymbol{m}^* \times \boldsymbol{m}^{n+1}) = \frac{\mu}{\chi_0} \frac{1}{\tau} (\chi(\Phi^*) \boldsymbol{h}^{n+1}, \boldsymbol{m}^{n+1}).$$

Multiplying Q^{n+1} on (3.10), we obtain

$$\begin{split} &\frac{1}{4\delta t}(|Q^{n+1}|^2 - |Q^n|^2 + |2Q^{n+1} - Q^n|^2 - |2Q^n - Q^{n-1}|^2 + |Q^{n+1} - Q^*|^2) \\ &= Q^{n+1}((\boldsymbol{u}^* \cdot \nabla)\boldsymbol{u}^*, \tilde{\boldsymbol{u}}^{n+1}) - Q^{n+1}(\boldsymbol{u}^*\Phi^*, \nabla W^{n+1}) + Q^{n+1}(\Phi^*\nabla W^*, \tilde{\boldsymbol{u}}^{n+1}) \\ &+ Q^{n+1}\mu((\tilde{\boldsymbol{u}}^{n+1} \cdot \nabla)\boldsymbol{m}^*, \nabla \varphi^*) + Q^{n+1}\mu((\nabla \cdot \tilde{\boldsymbol{u}}^{n+1})\boldsymbol{m}^*, \nabla \varphi^*) \\ &- Q^{n+1}\mu((\boldsymbol{u}^* \cdot \nabla)\boldsymbol{m}^*, \nabla \varphi^{n+1}) - Q^{n+1}\frac{\mu}{2}(\boldsymbol{m}^* \times \nabla \varphi^*, \nabla \times \tilde{\boldsymbol{u}}^{n+1}) \\ &+ Q^{n+1}\frac{\mu}{2}(\nabla \times \boldsymbol{u}^* \times \boldsymbol{m}^*, \nabla \varphi^{n+1}) + Q^{n+1}\frac{\mu}{\chi_0}((\boldsymbol{u}^* \cdot \nabla)\boldsymbol{m}^*, \boldsymbol{m}^{n+1}) \\ &- Q^{n+1}\frac{\mu}{\chi_0}\frac{1}{2}(\nabla \times \boldsymbol{u}^*, \boldsymbol{m}^* \times \boldsymbol{m}^{n+1}) - Q^{n+1}\frac{\mu}{\chi_0}\beta(\boldsymbol{m}^* \times \boldsymbol{h}^*, \boldsymbol{m}^* \times \boldsymbol{m}^{n+1}). \end{split}$$

The combination of (3.17) and (3.19)–(3.22) leads to

$$\begin{split} &\frac{\lambda \epsilon}{4\delta t} (\|\nabla \Phi^{n+1}\|^2 - \|\nabla \Phi^n\|^2 + \|2\nabla \Phi^{n+1} \\ &- \nabla \Phi^n\|^2 - \|2\nabla \Phi^n - \nabla \Phi^{n-1}\|^2 + \|\nabla \Phi^{n+1} - \nabla \Phi^*\|^2) \\ &+ \frac{S\lambda}{4\delta t \epsilon} (\|\Phi^{n+1}\|^2 - \|\Phi^n\|^2 + \|2\Phi^{n+1} - \Phi^n\|^2 - \|2\Phi^n - \Phi^{n-1}\|^2 + \|\Phi^{n+1} - \Phi^*\|^2) \\ &+ \frac{\lambda}{2\delta t} (\|U^{n+1}\|^2 - \|U^n\|^2 + \|2U^{n+1} - U^n\|^2 - \|2U^n - U^{n-1}\|^2 + \|U^{n+1} - U^*\|^2) \\ &+ \frac{1}{2\delta t} (3\tilde{u}^{n+1} - 4u^n + u^{n-1}, \tilde{u}^{n+1}) + \left\|\sqrt{\nu(\Phi^*)}D(\tilde{u}^{n+1})\right\|^2 + (\nabla p^n, \tilde{u}^{n+1}) \\ &+ \frac{\mu}{4\delta t} (\|h^{n+1}\|^2 - \|h^n\|^2 + \|2h^{n+1} - h^n\|^2 - \|2h^n - h^{n-1}\|^2 + \|h^{n+1} - h^*\|^2) \\ &+ \frac{1}{4\delta t} \frac{\mu}{\chi_0} (\|m^{n+1}\|^2 - \|m^n\|^2 \\ &+ \|2m^{n+1} - m^n\|^2 - \|2m^n - m^{n-1}\|^2 + \|m^{n+1} - m^*\|^2) \\ &+ M\|\nabla W^{n+1}\|^2 + \frac{\mu}{\tau} \|h^{n+1}\|^2 + \frac{\mu}{\tau} \|\sqrt{\chi(\Phi^*)}h^{n+1}\|^2 \\ &+ \mu\beta \|m^* \times h^{n+1}\|^2 + \frac{\mu}{\tau} \|m^{n+1}\|^2 \\ &+ \frac{1}{4\delta t} (|Q^{n+1}|^2 - |Q^n|^2 + |2Q^{n+1} - Q^n|^2 - |2Q^n - Q^{n-1}|^2 + |Q^{n+1} - Q^*|^2) \\ &= \mu(h_b^{n+1}, h^{n+1}) + \frac{\mu}{\tau} (h_a^{n+1}, h^{n+1}) + \frac{\mu}{\chi_0} \frac{1}{\tau} (\chi(\Phi^*) h^{n+1}, m^{n+1}). \end{split}$$

From (3.7) and (3.12), we derive the following orthogonal identity:

$$(3.24) \qquad \qquad (\boldsymbol{u}^{n+1} - \tilde{\boldsymbol{u}}^{n+1}, \boldsymbol{u}^{n+1}) = -\frac{2}{3}\delta t(\nabla p^{n+1} - \nabla p^n, \boldsymbol{u}^{n+1}) = 0.$$

Using (3.24), we derive

$$(3\tilde{\boldsymbol{u}}^{n+1} - 4\boldsymbol{u}^{n} + \boldsymbol{u}^{n-1}, \tilde{\boldsymbol{u}}^{n+1})$$

$$= (3\boldsymbol{u}^{n+1} - 4\boldsymbol{u}^{n} + \boldsymbol{u}^{n-1}, \tilde{\boldsymbol{u}}^{n+1}) + (3\tilde{\boldsymbol{u}}^{n+1} - 3\boldsymbol{u}^{n+1}, \tilde{\boldsymbol{u}}^{n+1})$$

$$= (3\boldsymbol{u}^{n+1} - 4\boldsymbol{u}^{n} + \boldsymbol{u}^{n-1}, \boldsymbol{u}^{n+1}) + (3\tilde{\boldsymbol{u}}^{n+1} - 3\boldsymbol{u}^{n+1}, \tilde{\boldsymbol{u}}^{n+1} + \boldsymbol{u}^{n+1})$$

$$= \frac{1}{2}(\|\boldsymbol{u}^{n+1}\|^{2} - \|\boldsymbol{u}^{n}\|^{2} + \|2\boldsymbol{u}^{n+1} - \boldsymbol{u}^{n}\|^{2} - \|2\boldsymbol{u}^{n} - \boldsymbol{u}^{n-1}\|^{2} + \|\boldsymbol{u}^{n+1} - \boldsymbol{u}^{*}\|^{2})$$

$$+ 3\|\tilde{\boldsymbol{u}}^{n+1}\|^{2} - 3\|\boldsymbol{u}^{n+1}\|^{2}$$

and

$$\begin{aligned} (3.26) \\ \|\tilde{\boldsymbol{u}}^{n+1}\|^2 - \|\boldsymbol{u}^{n+1}\|^2 &= (\tilde{\boldsymbol{u}}^{n+1} - \boldsymbol{u}^{n+1}, \tilde{\boldsymbol{u}}^{n+1} + \boldsymbol{u}^{n+1}) = (\tilde{\boldsymbol{u}}^{n+1} - \boldsymbol{u}^{n+1}, \tilde{\boldsymbol{u}}^{n+1} - \boldsymbol{u}^{n+1}) \\ &= \|\tilde{\boldsymbol{u}}^{n+1} - \boldsymbol{u}^{n+1}\|^2. \end{aligned}$$

We rewrite (3.7) as

(3.27)
$$\boldsymbol{u}^{n+1} + \frac{2}{3}\delta t \nabla p^{n+1} = \tilde{\boldsymbol{u}}^{n+1} + \frac{2}{3}\delta t \nabla p^{n}.$$

By taking the L^2 inner product of the above equation with itself, and using (3.12), we derive

$$(3.28) \quad (\tilde{\boldsymbol{u}}^{n+1}, \nabla p^n) = \frac{3}{4\delta t} \|\boldsymbol{u}^{n+1}\|^2 - \frac{3}{4\delta t} \|\tilde{\boldsymbol{u}}^{n+1}\|^2 + \frac{\delta t}{3} \|\nabla p^{n+1}\|^2 - \frac{\delta t}{3} \|\nabla p^n\|^2.$$

The combination of (3.25), (3.26), and (3.28) leads to

$$\begin{split} \frac{1}{2\delta t} (3\tilde{\boldsymbol{u}}^{n+1} - 4\boldsymbol{u}^n + \boldsymbol{u}^{n-1}, \tilde{\boldsymbol{u}}^{n+1}) + (\tilde{\boldsymbol{u}}^{n+1}, \nabla p^n) \\ (3.29) &= \frac{1}{4\delta t} (\|\boldsymbol{u}^{n+1}\|^2 - \|\boldsymbol{u}^n\|^2 + \|2\boldsymbol{u}^{n+1} - \boldsymbol{u}^n\|^2 - \|2\boldsymbol{u}^n - \boldsymbol{u}^{n-1}\|^2 + \|\boldsymbol{u}^{n+1} - \boldsymbol{u}^*\|^2) \\ &+ \frac{3}{4\delta t} \|\boldsymbol{u}^{n+1} - \tilde{\boldsymbol{u}}^{n+1}\|^2 + \frac{\delta t}{3} \|\nabla p^{n+1}\|^2 - \frac{\delta t}{3} \|\nabla p^n\|^2. \end{split}$$

Furthermore, we combine (3.23) and (3.29) to deduce

(3.30)

$$\begin{split} &\frac{\lambda\epsilon}{4\delta t}(\|\nabla\Phi^{n+1}\|^2 - \|\nabla\Phi^n\|^2 + \|2\nabla\Phi^{n+1} - \nabla\Phi^n\|^2 \\ &- \|2\nabla\Phi^n - \nabla\Phi^{n-1}\|^2 + \|\nabla\Phi^{n+1} - \nabla\Phi^*\|^2) \\ &+ \frac{S\lambda}{4\delta t\epsilon}(\|\Phi^{n+1}\|^2 - \|\Phi^n\|^2 + \|2\Phi^{n+1} - \Phi^n\|^2 - \|2\Phi^n - \Phi^{n-1}\|^2 + \|\Phi^{n+1} - \Phi^*\|^2) \\ &+ \frac{\lambda}{2\delta t}(\|U^{n+1}\|^2 - \|U^n\|^2 + \|2U^{n+1} - U^n\|^2 - \|2U^n - U^{n-1}\|^2 + \|U^{n+1} - U^*\|^2) \\ &+ \frac{1}{4\delta t}(\|u^{n+1}\|^2 - \|u^n\|^2 + \|2u^{n+1} - u^n\|^2 - \|2u^n - u^{n-1}\|^2 + \|u^{n+1} - u^*\|^2) \\ &+ \frac{\mu}{4\delta t}(\|h^{n+1}\|^2 - \|h^n\|^2 + \|2h^{n+1} - h^n\|^2 - \|2h^n - h^{n-1}\|^2 + \|h^{n+1} - h^*\|^2) \\ &+ \frac{1}{4\delta t}\frac{\mu}{\chi_0}(\|m^{n+1}\|^2 - \|m^n\|^2 + \|2m^{n+1} - m^n\|^2 \\ &- \|2m^n - m^{n-1}\|^2 + \|m^{n+1} - m^*\|^2) \\ &+ \frac{1}{4\delta t}(|Q^{n+1}|^2 - |Q^n|^2 + |2Q^{n+1} - Q^n|^2 - |2Q^n - Q^{n-1}|^2 + |Q^{n+1} - Q^*|^2) \\ &+ \frac{\delta t}{3}\|\nabla p^{n+1}\|^2 - \frac{\delta t}{3}\|\nabla p^n\|^2 + \frac{3}{4\delta t}\|u^{n+1} - \tilde{u}^{n+1}\|^2 + \left\|\sqrt{\nu(\Phi^*)}D(\tilde{u}^{n+1})\right\|^2 \\ &+ \mu\beta\|m^* \times h^{n+1}\|^2 + \frac{\mu}{\tau}\|h^{n+1}\|^2 + \frac{\mu}{\tau}\|\sqrt{\chi(\Phi^*)}h^{n+1}\|^2 \\ &= \mu(h_b^{n+1}, h^{n+1}) + \frac{\mu}{\tau}(h_a^{n+1}, h^{n+1}) + \frac{\mu}{\tau\chi_0}(\chi(\Phi^*)h^{n+1}, m^{n+1}). \end{split}$$

The terms on the right-hand side can be estimated as

$$(3.31) \qquad \frac{\mu}{\tau \chi_0} (\chi(\Phi^*) \boldsymbol{h}^{n+1}, \boldsymbol{m}^{n+1}) \leq \frac{\mu}{\tau} \| \sqrt{\chi(\Phi^*)} \boldsymbol{h}^{n+1} \|^2 + \frac{\mu}{4\tau \chi_0} \| \boldsymbol{m}^{n+1} \|^2$$

and

$$(3.32) \\ \frac{\mu}{\tau}(\boldsymbol{h}_{a}^{n+1}, \boldsymbol{h}^{n+1}) + \mu(\boldsymbol{h}_{b}^{n+1}, \boldsymbol{h}^{n+1}) \\ \leq \frac{\mu}{4\tau} \|\boldsymbol{h}^{n+1}\|^{2} + \frac{\mu}{\tau} \|\boldsymbol{h}_{a}^{n+1}\|^{2} + \frac{\mu}{4\tau} \|\boldsymbol{h}^{n+1}\|^{2} + \tau\mu \|\boldsymbol{h}_{b}^{n+1}\|^{2}.$$

Thus, using (3.31) and (3.32), and dropping several unnecessary positive terms, we finish the proof.

3.2. Fully decoupled implementation. Formally, the scheme (3.2)–(3.10) seems to be a coupled algorithm, but in fact it can achieve a fully decoupled manner by splitting the variables using the scalar variable Q, as discussed below.

We split the unknowns Φ , W, $\tilde{\boldsymbol{u}}$, φ , and \boldsymbol{m} into the following form:

$$\begin{cases} \Phi^{n+1} = \Phi_1^{n+1} + Q^{n+1}\Phi_2^{n+1}, W^{n+1} = W_1^{n+1} + Q^{n+1}W_2^{n+1}, \\ \tilde{\boldsymbol{u}}^{n+1} = \tilde{\boldsymbol{u}}_1^{n+1} + Q^{n+1}\tilde{\boldsymbol{u}}_2^{n+1}, \\ \varphi^{n+1} = \varphi_1^{n+1} + Q^{n+1}\varphi_2^{n+1}, \boldsymbol{m}^{n+1} = \boldsymbol{m}_1^{n+1} + Q^{n+1}\boldsymbol{m}_2^{n+1}, \end{cases}$$

where $(\Phi_i^{n+1}, W_i^{n+1}) \in Y_h^2$, $\tilde{\boldsymbol{u}}_i^{n+1} \in \boldsymbol{V}_h$, $\varphi_i^{n+1} \in \Psi_h$, and $\boldsymbol{m}_i^{n+1} \in \boldsymbol{N}_h$ for $i=1,\ 2$.

By substituting (3.4) into (3.3), and using (3.33) and the scalar feature of Q^{n+1} , we can split (3.2)–(3.3) into the following two substeps.

Step 1. Find $(\Phi_1^{n+1}, W_1^{n+1}) \in Y_h^2$ such that for all $(\Lambda, X) \in Y_h^2$,

$$\begin{cases} (3.34) \\ \begin{cases} \frac{3}{2\delta t}(\Phi_1^{n+1}, \Lambda) + M(\nabla W_1^{n+1}, \nabla \Lambda) = (f_1^1, \Lambda), \\ (W_1^{n+1}, X) = \lambda \epsilon (\nabla \Phi_1^{n+1}, \nabla X) + \frac{\lambda}{2} \left(H(\Phi^*) \Phi_1^{n+1}, H(\Phi^*) X \right) + \frac{S\lambda}{\epsilon} (\Phi_1^{n+1}, X) + (f_2^1, X), \end{cases}$$

where

$$\begin{split} &(f_1^1,\Lambda) = \frac{1}{2\delta t}(4\Phi^n - \Phi^{n-1},\Lambda),\\ &(f_2^1,X) = -\frac{2}{3}\lambda\left(H(\Phi^*)^2\Phi^n,X\right) + \frac{\lambda}{6}\left(H(\Phi^*)^2\Phi^{n-1},X\right) + \frac{4}{3}\lambda\left(H(\Phi^*)U^n,X\right) \\ &-\frac{\lambda}{3}\left(H(\Phi^*)U^{n-1},X\right). \end{split}$$

Step 2. Find $(\Phi_2^{n+1}, W_2^{n+1}) \in Y_h^2$ such that for all $(\Lambda, X) \in Y_h^2$,

$$\begin{cases} \frac{3}{2\delta t}(\Phi_2^{n+1},\Lambda) + M(\nabla W_2^{n+1},\nabla \Lambda) = (\boldsymbol{u}^*\Phi^*,\nabla \Lambda), \\ (W_2^{n+1},X) = \lambda \epsilon(\nabla \Phi_2^{n+1},\nabla X) + \frac{\lambda}{2}\left(H(\Phi^*)\Phi_2^{n+1},H(\Phi^*)X\right) + \frac{S\lambda}{\epsilon}(\Phi_2^{n+1},X). \end{cases}$$

By taking (3.33) into (3.5), then (3.5) can be decomposed into two substeps as follows.

Step 3. Find $\tilde{\boldsymbol{u}}_1^{n+1} \in \boldsymbol{V}_h$ such that for all $\boldsymbol{v} \in \boldsymbol{V}_h$,

$$(3.36) \qquad \qquad \frac{3}{2\delta t}(\tilde{\boldsymbol{u}}_1^{n+1}, \boldsymbol{v}) + (\nu(\Phi^*)D(\tilde{\boldsymbol{u}}_1^{n+1}), D(\boldsymbol{v})) = (\boldsymbol{f}^3, \boldsymbol{v}),$$

 $\begin{array}{l} \text{where } (\boldsymbol{f}^3,\boldsymbol{v}) = \frac{1}{2\delta t}(4\boldsymbol{u}^n - \boldsymbol{u}^{n-1},\boldsymbol{v}) - (\nabla p^n,\boldsymbol{v}). \\ Step \ 4. \ \text{Find} \ \boldsymbol{\tilde{u}}_2^{n+1} \in \boldsymbol{V}_h \ \text{such that for all} \ \boldsymbol{v} \in \boldsymbol{V}_h, \end{array}$

(3.37)
$$\frac{3}{2\delta t}(\tilde{\boldsymbol{u}}_2^{n+1}, \boldsymbol{v}) + (\nu(\Phi^*)D(\tilde{\boldsymbol{u}}_2^{n+1}), D(\boldsymbol{v})) = (\boldsymbol{f}^4, \boldsymbol{v}),$$

where $(\boldsymbol{f}^4, \boldsymbol{v}) = -((\boldsymbol{u}^* \cdot \nabla) \boldsymbol{u}^*, \boldsymbol{v}) - (\Phi^* \nabla W^*, \boldsymbol{v}) - \mu((\boldsymbol{v} \cdot \nabla) \boldsymbol{m}^*, \boldsymbol{h}^*) - \mu((\nabla \cdot \boldsymbol{v}) \boldsymbol{m}^*, \boldsymbol{h}^*) + \frac{\mu}{2} (\boldsymbol{m}^* \times \boldsymbol{h}^*, \nabla \times \boldsymbol{v}).$

By taking (3.33) into (3.8), we decouple the obtained equation into two substeps as follows.

Step 5. Find $\varphi_1^{n+1} \in \Psi_h$ such that for all $\psi \in \Psi_h$

(3.38)
$$\frac{3}{2\delta t} (\nabla \varphi_1^{n+1}, \nabla \psi) + \frac{1}{\tau} (\nabla \varphi_1^{n+1}, \nabla \psi) + \frac{1}{\tau} (\chi(\Phi^*) \nabla \varphi_1^{n+1}, \nabla \psi) + \beta (\boldsymbol{m}^* \times \nabla \varphi_1^{n+1}, \boldsymbol{m}^* \times \nabla \psi) = (\boldsymbol{f}^5, \nabla \psi),$$

where $(\boldsymbol{f}^5, \nabla \psi) = (\boldsymbol{h}_b^{n+1}, \nabla \psi) + \frac{1}{\tau}(\boldsymbol{h}_a^{n+1}, \nabla \psi) + \frac{1}{2\delta t}(4\nabla \varphi^n - \nabla \varphi^{n-1}, \nabla \psi)$. Step 6. Find $\varphi_2^{n+1} \in \Psi_h$ such that for all $\psi \in \Psi_h$,

$$(3.39)$$

$$\frac{3}{2\delta t}(\nabla \varphi_2^{n+1}, \nabla \psi) + \frac{1}{\tau}(\nabla \varphi_2^{n+1}, \nabla \psi) + \frac{1}{\tau}(\chi(\Phi^*) \nabla \varphi_2^{n+1}, \nabla \psi) + \beta(\boldsymbol{m}^* \times \nabla \varphi_2^{n+1}, \boldsymbol{m}^* \times \nabla \psi) = (\boldsymbol{f}^6, \nabla \psi),$$

where $(\boldsymbol{f}^6, \nabla \psi) = ((\boldsymbol{u}^* \cdot \nabla) \boldsymbol{m}^*, \nabla \psi) - \frac{1}{2} (\nabla \times \boldsymbol{u}^*, \boldsymbol{m}^* \times \nabla \psi).$ By taking (3.33) into (3.9), and using $\boldsymbol{h}_i^{n+1} = \nabla \varphi_i^{n+1}, \ i = 1, 2, \ (3.9)$ can be partitioned into two substeps as follows.

Step 7. Find $m_1^{n+1} \in N_h$ such that for all $n \in N_h$,

(3.40)
$$\frac{3}{2\delta t}(\boldsymbol{m}_{1}^{n+1},\boldsymbol{n}) + \frac{1}{\tau}(\boldsymbol{m}_{1}^{n+1},\boldsymbol{n}) = (\boldsymbol{f}^{7},\boldsymbol{n}),$$

where $(\boldsymbol{f}^7, \boldsymbol{n}) = \frac{1}{\tau} (\chi(\Phi^*) \boldsymbol{h}_1^{n+1}, \boldsymbol{n}) + \frac{1}{2\delta t} (4\boldsymbol{m}^n - \boldsymbol{m}^{n-1}, \boldsymbol{n}).$ Step 8. Find $\boldsymbol{m}_2^{n+1} \in \boldsymbol{N}_h$ such that for all $\boldsymbol{n} \in \boldsymbol{N}_h$,

(3.41)
$$\frac{3}{2\delta t}(\boldsymbol{m}_{2}^{n+1},\boldsymbol{n}) + \frac{1}{\tau}(\boldsymbol{m}_{2}^{n+1},\boldsymbol{n}) = (\boldsymbol{f}^{8},\boldsymbol{n}),$$

where $(\boldsymbol{f}^8, \boldsymbol{n}) = -((\boldsymbol{u}^* \cdot \nabla)\boldsymbol{m}^*, \boldsymbol{n}) + \frac{1}{2}(\nabla \times \boldsymbol{u}^*, \boldsymbol{m}^* \times \boldsymbol{n}) + \beta(\boldsymbol{m}^* \times \boldsymbol{h}^*, \boldsymbol{m}^* \times \boldsymbol{n}) +$

To solve Q^{n+1} , we use (3.33) to rewrite (3.10) as the following step. Step 9.

(3.42)
$$Q^{n+1} = \frac{2\delta t \eta_1 + 4Q^n - Q^{n-1}}{3 - 2\delta t \eta_2},$$

where for i = 1, 2

$$\begin{split} &\eta_i = ((\boldsymbol{u}^* \cdot \nabla) \boldsymbol{u}^*, \tilde{\boldsymbol{u}}_i^{n+1}) - (\boldsymbol{u}^* \boldsymbol{\Phi}^*, \nabla W_i^{n+1}) + (\boldsymbol{\Phi}^* \nabla W^*, \tilde{\boldsymbol{u}}_i^{n+1}) \\ &+ \mu((\tilde{\boldsymbol{u}}_i^{n+1} \cdot \nabla) \boldsymbol{m}^*, \nabla \varphi^*) + \mu((\nabla \cdot \tilde{\boldsymbol{u}}_i^{n+1}) \boldsymbol{m}^*, \nabla \varphi^*) - \mu((\boldsymbol{u}^* \cdot \nabla) \boldsymbol{m}^*, \nabla \varphi_i^{n+1}) \\ &- \frac{\mu}{2} (\boldsymbol{m}^* \times \nabla \varphi^*, \nabla \times \tilde{\boldsymbol{u}}_i^{n+1}) + \frac{\mu}{2} (\nabla \times \boldsymbol{u}^*, \boldsymbol{m}^* \times \nabla \varphi_i^{n+1}) + \frac{\mu}{\chi_0} ((\boldsymbol{u}^* \cdot \nabla) \boldsymbol{m}^*, \boldsymbol{m}_i^{n+1}) \\ &- \frac{\mu}{\gamma_0} \frac{1}{2} (\nabla \times \boldsymbol{u}^*, \boldsymbol{m}^* \times \boldsymbol{m}_i^{n+1}) - \frac{\mu}{\gamma_0} \beta(\boldsymbol{m}^* \times \boldsymbol{h}^*, \boldsymbol{m}^* \times \boldsymbol{m}_i^{n+1}). \end{split}$$

After solving Steps 1–9, we could update all unknowns by the following step.

Step 10. The variables Φ^{n+1} , W^{n+1} , \tilde{u}^{n+1} , φ^{n+1} , and m^{n+1} can be updated by using (3.33); the pressure p^{n+1} can be updated by (3.6), and u^{n+1} is updated by using (3.7); the auxiliary variable U^{n+1} is finally updated by using (3.11).

In the following theorem, we show the well-posedness of the decoupled problems (3.34)-(3.42).

Theorem 3.2. The decoupled problems (3.34)-(3.42) in Steps 1-10 are uniquely solvable.

Proof. The uniquely solvability of (3.34)–(3.35) in Steps 1–2 can be shown by using the Lax-Milgram theorem; cf. [60]. The well-posedness of (3.36)-(3.37) in Steps 3–4 can be obtained using Korn's inequality; cf. [4]. The well-posedness of (3.38)–(3.39) in Steps 5–6 involves the property of symmetric positive definite operator, which is easily obtained. The coercivity of (3.40)–(3.41) in Steps 7–8 can be derived using the inverse inequality (cf. [4]), that is,

$$(3.43) \qquad \frac{3}{2\delta t}(\bm{m}, \bm{m}) + \frac{1}{\tau}(\bm{m}, \bm{m}) = \left(\frac{3}{2\delta t} + \frac{1}{\tau}\right) \|\bm{m}\|^2 \ge ch^2 \left(\frac{3}{2\delta t} + \frac{1}{\tau}\right) \|\bm{m}\|_{1}^2,$$

which deduces the well-posedness.

We finally prove the solvability of Step 9 as follows by showing $3-2\delta t\eta_2\neq 0$. By taking $\Lambda=W_2^{n+1},\ X=\frac{3}{2\delta t}\Phi_2^{n+1}$ in (3.35), we obtain

$$\begin{cases} \frac{3}{2\delta t}(\Phi_2^{n+1},W_2^{n+1}) + M\|\nabla W_2^{n+1}\|^2 = (\boldsymbol{u}^*\Phi^*,\nabla W_2^{n+1}),\\ \frac{3}{2\delta t}(W_2^{n+1},\Phi_2^{n+1}) = \frac{3}{2\delta t}\lambda\epsilon\|\nabla\Phi_2^{n+1}\|^2 + \frac{3}{2\delta t}\frac{\lambda}{2}\|H(\Phi^*)\Phi_2^{n+1}\|^2 + \frac{3}{2\delta t}\frac{S\lambda}{\epsilon}\|\Phi_2^{n+1}\|^2, \end{cases}$$

which yields

$$\begin{split} A_1 &= (\boldsymbol{u}^* \Phi^*, \nabla W_2^{n+1}) = M \|\nabla W_2^{n+1}\|^2 + \frac{3}{2\delta t} \lambda \epsilon \|\nabla \Phi_2^{n+1}\|^2 \\ &+ \frac{3}{2\delta t} \frac{\lambda}{2} \|H(\Phi^*) \Phi_2^{n+1}\|^2 + \frac{3}{2\delta t} \frac{S\lambda}{\epsilon} \|\Phi_2^{n+1}\|^2 \geq 0. \end{split}$$

By taking $\tilde{\boldsymbol{u}}_{2}^{n+1}$ in (3.37), we have

$$\begin{split} A_2 &= -((\boldsymbol{u}^* \cdot \nabla) \boldsymbol{u}^*, \tilde{\boldsymbol{u}}_2^{n+1}) \\ &- (\Phi^* \nabla W^*, \tilde{\boldsymbol{u}}_2^{n+1}) - \mu((\tilde{\boldsymbol{u}}_2^{n+1} \cdot \nabla) \boldsymbol{m}^*, \boldsymbol{h}^*) - \mu((\nabla \cdot \tilde{\boldsymbol{u}}_2^{n+1}) \boldsymbol{m}^*, \boldsymbol{h}^*) \\ &+ \frac{\mu}{2} (\boldsymbol{m}^* \times \boldsymbol{h}^*, \nabla \times \tilde{\boldsymbol{u}}_2^{n+1}) = \frac{3}{2\delta t} \|\tilde{\boldsymbol{u}}_2^{n+1}\|^2 + \left\| \sqrt{\nu(\Phi^*)} D(\tilde{\boldsymbol{u}}_2^{n+1}) \right\|^2 \geq 0. \end{split}$$

By taking $\psi = \mu \varphi_2^{n+1}$ in (3.39), we get

$$\begin{split} A_3 &= \mu \left((\boldsymbol{u}^* \cdot \nabla) \boldsymbol{m}^*, \nabla \varphi_2^{n+1} \right) - \frac{\mu}{2} (\nabla \times \boldsymbol{u}^*, \boldsymbol{m}^* \times \nabla \varphi_2^{n+1} \right) \\ &= \frac{3\mu}{2\delta t} \|\nabla \varphi_2^{n+1}\|^2 + \frac{\mu}{\tau} \|\nabla \varphi_2^{n+1}\|^2 + \frac{\mu}{\tau} \left\| \sqrt{\chi(\Phi^*)} \nabla \varphi_2^{n+1} \right\|^2 + \mu\beta \|\boldsymbol{m}^* \times \nabla \varphi_2^{n+1}\|^2. \end{split}$$

By taking $\boldsymbol{n} = \frac{\mu}{\chi_0} \boldsymbol{m}_2^{n+1}$ in (3.41), we get

$$\begin{split} A_4 &= -\frac{\mu}{\chi_0} \left((\boldsymbol{u}^* \cdot \nabla) \boldsymbol{m}^*, \boldsymbol{m}_2^{n+1} \right) + \frac{\mu}{\chi_0} \frac{1}{2} \left(\nabla \times \boldsymbol{u}^*, \boldsymbol{m}^* \times \boldsymbol{m}_2^{n+1} \right) \\ &+ \frac{\mu}{\chi_0} \beta \left(\boldsymbol{m}^* \times \boldsymbol{h}^*, \boldsymbol{m}^* \times \boldsymbol{m}_2^{n+1} \right) \\ &= \frac{\mu}{\chi_0} \frac{3}{2\delta t} \| \boldsymbol{m}_2^{n+1} \|^2 + \frac{\mu}{\chi_0} \frac{1}{\tau} \| \boldsymbol{m}_2^{n+1} \|^2 - \frac{\mu}{\chi_0} \frac{1}{\tau} \left(\chi(\Phi^*) \boldsymbol{h}_2^{n+1}, \boldsymbol{m}_2^{n+1} \right). \end{split}$$

Using the Cauchy–Schwarz inequality, we estimate the last term of A_4 as

$$\begin{split} \frac{\mu}{\tau \chi_0} | \left(\chi(\Phi^*) \boldsymbol{h}_2^{n+1}, \boldsymbol{m}_2^{n+1} \right) | &\leq \frac{\mu}{\tau \chi_0} \left\| \sqrt{\chi(\Phi^*)} \boldsymbol{h}_2^{n+1} \right\| \left\| \sqrt{\chi(\Phi^*)} \boldsymbol{m}_2^{n+1} \right\| \\ &\leq \frac{\mu}{\tau} \left\| \sqrt{\chi(\Phi^*)} \boldsymbol{h}_2^{n+1} \right\|^2 + \frac{\mu}{4\tau \chi_0} \| \boldsymbol{m}_2^{n+1} \|^2. \end{split}$$

Thus, we derive

$$\begin{split} A_3 + A_4 &\geq \frac{3\mu}{2\delta t} \|\nabla \varphi_2^{n+1}\|^2 + \frac{\mu}{\tau} \|\nabla \varphi_2^{n+1}\|^2 + \mu\beta \|\boldsymbol{m}^* \times \nabla \varphi_2^{n+1}\|^2 \\ &+ \frac{\mu}{\chi_0} \frac{3}{2\delta t} \|\boldsymbol{m}_2^{n+1}\|^2 + \frac{3\mu}{4\chi_0 \tau} \|\boldsymbol{m}_2^{n+1}\|^2 \geq 0. \end{split}$$

Therefore, we obtain $-\eta_2 = A_1 + A_2 + A_3 + A_4 \ge 0$, which implies the solvability of (3.42) in Step 9. The proof of unique solvability of Steps 1–10 is completed.

So far, we have constructed the desired scheme (3.2)–(3.10) for the two-phase FHD model (2.3)–(2.10); i.e., a linear, fully decoupled, second-order accurate in time, unconditionally energy stable numerical algorithm based on the continuous finite element discretizations is obtained. Furthermore, our algorithm is very efficient because it decomposes the coupled nonlinear saddle point system into multiple independent elliptic problems.

4. Numerical simulations. In this section, we carry out a series of 2D and 3D numerical simulations to verify the accuracy and stability of our scheme and exhibit some interesting and iconic "spiking" phenomena of ferrofluids under some specific applied magnetic fields. The continuous (conforming) finite elements are applied for spatial discretization, where the first-order (linear) polynomials are used for V_h , Q_h , and N_h and second-order (quadratic) polynomials are used for V_h and Ψ_h .

We denote $e_w = w(t_n, \mathbf{x}) - w^n$, which is the approximation error at $t = t_n$, and " \lesssim " the relation of $a \leq Cb$ for some constant C. Using the selected finite element spaces, the scheme we developed expects the following error estimates:

$$\|e_{\Phi}\|_{L^2} + \|e_{h}\|_{L^2} + \|e_{m}\|_{L^2} \lesssim \delta t^2 + h^2, \quad \|e_{u}\|_{L^2} \lesssim \delta t^2 + h^3, \quad \|e_{\Phi}\|_{H^1} \lesssim \delta t^2 + h.$$

Meanwhile, note that the L^2 error of p and the H^1 error of u are not full second-order accuracy using the pressure projection method due to the artificial Neumann boundary condition imposed on the pressure; see [39].

The applied magnetic field h_a is generated by a linear combination of dipoles that reads as

$$oldsymbol{h}_a = \sum_s lpha_s
abla \phi_s(oldsymbol{x}), \ \phi_s(oldsymbol{x}) = rac{oldsymbol{d} \cdot (oldsymbol{x}_s - oldsymbol{x})}{|oldsymbol{x}_s - oldsymbol{x}|^2},$$

where $|\mathbf{d}| = 1$ indicates the direction of the dipole, and \mathbf{x}_s is the dipole's position. It is easy to verify that \mathbf{h}_a is a harmonic field (i.e., $\nabla \times \mathbf{h}_a = \mathbf{0}$, $\nabla \cdot \mathbf{h}_a = 0$); cf. [33].

4.1. Accuracy tests. We first verify the order of accuracy of our developed scheme in this subsection. We set the domain as $\Omega = [0,1]^2$ and assume that the exact solution of the FHD system (2.3)–(2.10) is

$$\begin{cases} \Phi(t, \boldsymbol{x}) &= 0.5 \sin(t) \cos(\pi x) \cos(\pi y) + 0.5, \\ \boldsymbol{u}(t, \boldsymbol{x}) &= \left(\sin(t) \sin(\pi x) \sin(\pi (y + 0.5)), \sin(t) \cos(\pi x) \cos(\pi (y + 0.5))\right), \\ p(t, \boldsymbol{x}) &= \sin(t) (2x - 1) (2y - 1), \varphi(t, \boldsymbol{x}) = (x - 0.5) y \sin(t), \\ \boldsymbol{m}(t, \boldsymbol{x}) &= \left(\sin(t + y), \sin(t + x)\right). \end{cases}$$

The model parameters are set as

$$\epsilon = 0.05, \ M = 0.05, \ \nu_f = 2, \ \nu_w = 1, \ \mu = \tau = \beta = \chi_0 = \lambda = 1, \ S = 1, \ B = 1 + \frac{S}{2\epsilon}.$$

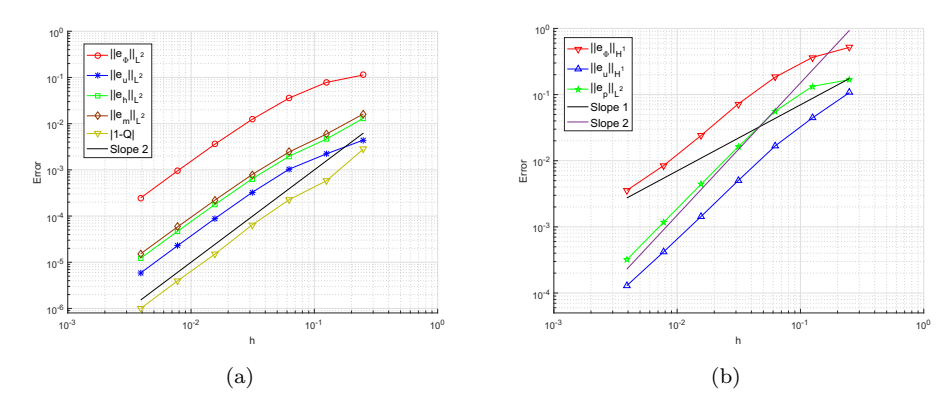


FIG. 4.1. Numerical errors computed by $\delta t = \frac{1}{2}h$, where (a) $||e_{\Phi}||$, $||e_{\boldsymbol{u}}||$, $||e_{\boldsymbol{h}}||$, $||e_{\boldsymbol{m}}||$, and |1-Q|, (b) $||e_{\Phi}||_1$, $||e_{\boldsymbol{u}}||_1$, and $||e_{\boldsymbol{p}}||$.

To observe the convergent orders, we set $\delta t = \frac{1}{2}h$. From (4.1), the optimal error estimates in term of h are expected to be

$$||e_{\Phi}||_{L^2} + ||e_{h}||_{L^2} + ||e_{m}||_{L^2} + ||e_{u}||_{L^2} \lesssim h^2, \quad ||e_{\Phi}||_{H^1} \lesssim h.$$

In Figure 4.1, the results of numerical errors and convergent orders at T=0.5 are plotted. We observe that the L^2 errors of Φ , \boldsymbol{u} , \boldsymbol{h} , and \boldsymbol{m} are second-order accurate, and the H^1 error of Φ is asymptotically first-order accurate, which are in line with the expected order. The orders of the L^2 error of p and the H^1 error of \boldsymbol{u} are higher than first-order accuracy, but not full second-order accuracy due to the artificial Neumann boundary condition for p, and the scalar variable Q approximates 1 with second-order accuracy as well.

4.2. Stability tests. In this subsection, we carry out the simulation of a benchmark problem of coarsening effects of two bubbles of the Cahn–Hilliard dynamics; cf. [6, 60]. The computational domain is set as $\Omega = [0, 2\pi]^2$, and the initial condition of Φ_0 is set as

$$\Phi_0(\mathbf{x}) = 1 - \frac{1}{2} \tanh \left(\frac{\sqrt{(x - x_1)^2 + (y - y_1)^2} - r_1}{1.2\epsilon} \right) - \frac{1}{2} \tanh \left(\frac{\sqrt{(x - x_2)^2 + (y - y_2)^2} - r_2}{1.2\epsilon} \right),$$

where $(x_1, y_1) = (\pi - 0.7, \pi - 0.6)$, $r_1 = 1.5$, $(x_2, y_2) = (\pi + 1.65, \pi + 1.6)$, $r_2 = 0.7$. All other variables including the applied magnetic field \mathbf{h}_a are all set zeros. The model parameters are set as

$$\begin{split} \epsilon &= 0.05, M = 5, \nu_f = 2, \nu_w = 1, \mu = \tau = \beta = \chi_0 = \lambda = 1, S = 1, \\ B &= \frac{S}{2\epsilon} + 10, h = \frac{1}{256}, \delta t = \frac{1}{100}. \end{split}$$

To illustrate the effectiveness of our developed scheme, we also compare with another implicit-explicit type scheme, which reads as follow: find $(\Phi^{n+1}, W^{n+1}, \boldsymbol{u}^{n+1}, p^{n+1}, \varphi^{n+1}, \boldsymbol{m}^{n+1}) \in Y_h^2 \times \boldsymbol{V}_h \times Q_h \times \Psi_h \times \boldsymbol{N}_h$ such that

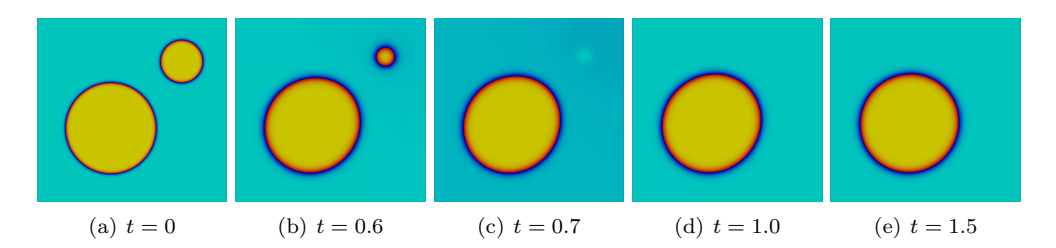


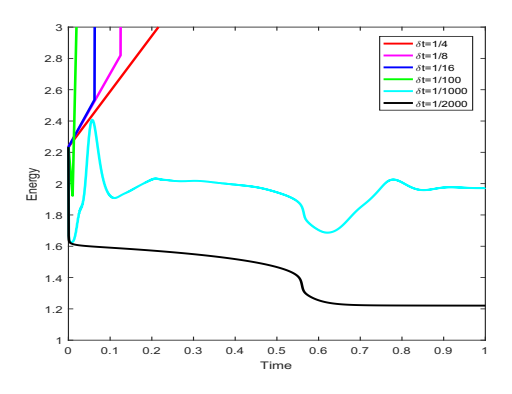
FIG. 4.2. The profiles of the phase-field variable Φ at various times computed by $\delta t = 0.01$ and $h = \frac{1}{256}$.

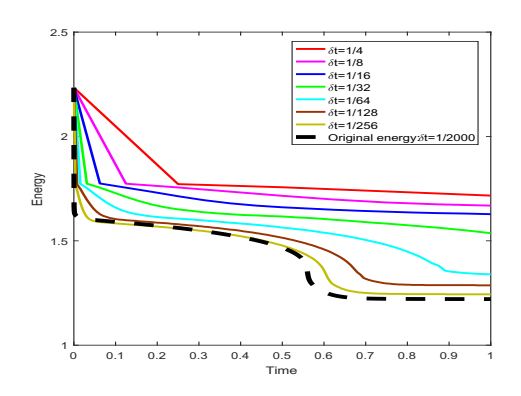
$$(4.2) \begin{cases} (D_{t}\Phi^{n+1}, \Lambda) - (\boldsymbol{u}^{*}\Phi^{*}, \nabla\Lambda) + M(\nabla W^{n+1}, \nabla\Lambda) = 0, \\ (W^{n+1}, X) = \lambda \epsilon(\nabla \Phi^{n+1}, \nabla X) + \lambda(f(\Phi^{*}), X), \\ (D_{t}\boldsymbol{u}^{n+1}, \boldsymbol{v}) + (\nu(\Phi^{*})D(\boldsymbol{u}^{n+1}), D(\boldsymbol{v})) - (p^{n+1}, \nabla \cdot \boldsymbol{v}) \\ + ((\boldsymbol{u}^{*} \cdot \nabla)\boldsymbol{u}^{*}, \boldsymbol{v}) + (\Phi^{*}\nabla W^{*}, \boldsymbol{v}) \\ = -\mu((\boldsymbol{v} \cdot \nabla)\boldsymbol{m}^{*}, \nabla \varphi^{*}) - \mu((\nabla \cdot \boldsymbol{v})\boldsymbol{m}^{*}, \nabla \varphi^{*}) + \frac{\mu}{2}(\boldsymbol{m}^{*} \times \nabla \varphi^{*}, \nabla \times \boldsymbol{v}), \\ (\nabla \cdot \boldsymbol{u}^{n+1}, q) = 0, \\ (\nabla D_{t}\varphi^{n+1}, \nabla \psi) + \frac{1}{\tau}(\nabla \varphi^{n+1}, \nabla \psi) + \frac{1}{\tau}(\chi(\Phi^{*})\nabla \varphi^{n+1}, \nabla \psi) - ((\boldsymbol{u}^{*} \cdot \nabla)\boldsymbol{m}^{*}, \nabla \psi) \\ + \frac{1}{2}(\nabla \times \boldsymbol{u}^{*} \times \boldsymbol{m}^{*}, \nabla \psi) + \beta(\boldsymbol{m}^{*} \times \nabla \varphi^{n+1}, \boldsymbol{m}^{*} \times \nabla \psi) \\ = (\boldsymbol{h}_{b}^{n+1}, \nabla \psi) + \frac{1}{\tau}(\boldsymbol{h}_{a}^{n+1}, \nabla \psi), \\ (D_{t}\boldsymbol{m}^{n+1}, \boldsymbol{n}) + ((\boldsymbol{u}^{*} \cdot \nabla)\boldsymbol{m}^{*}, \boldsymbol{n}) - \frac{1}{2}(\nabla \times \boldsymbol{u}^{*} \times \boldsymbol{m}^{*}, \boldsymbol{n}) \\ - \beta(\boldsymbol{m}^{*} \times \boldsymbol{h}^{*}, \boldsymbol{m}^{*} \times \boldsymbol{n}) + \frac{1}{\tau}(\boldsymbol{m}^{n+1}, \boldsymbol{n}) \\ = \frac{1}{\tau}(\chi(\Phi^{*})\boldsymbol{h}^{n+1}, \boldsymbol{n}) \end{cases}$$

for all $(\Lambda, X, \mathbf{v}, q, \psi, \mathbf{n}) \in Y_h^2 \times \mathbf{V}_h \times Q_h \times \Psi_h \times \mathbf{N}_h$. The idea behind developing this particular scheme is to explicitly discretize all nonlinear terms and implicitly discretize linear terms; see a similar scheme given in [24] for a relatively simple hydrodynamic coupled phase-field model (for viscous Newtonian fluid).

In Figure 4.2, we show snapshots of the phase-field variable Φ at different times, where the coarsening effect drives the gradual absorption of the small circle by the larger circle, and the total absorption occurs around t = 0.7. In Figure 4.3(a), we plot the temporal evolution of the original energy $E(\Phi, \boldsymbol{u}, \boldsymbol{h}, \boldsymbol{m})$ given in (2.11) computed by using the implicit-explicit scheme (4.2), where different time steps are used. We observe that the implicit-explicit scheme is energy stable conditionally. That is, for smaller time steps $\delta t \leq 1/2000$, it is energy stable, while for larger time steps, the energy curve explodes, meaning the energy evolution is unstable. In Figure 4.3(b), we plot the temporal energy evolution of \tilde{E}^{n+1} given in (3.13) computed by our developed scheme for different time step sizes, where the black dashed line is the original energy computed by the implicit-explicit scheme (4.2) with $\delta t = 1/2000$ as a reference. All computed energy curves of \tilde{E}^{n+1} show decays monotonically, which numerically confirms that our algorithm is unconditionally energy stable.

4.3. Rosensweig instability in two and three dimensions. In this subsection, we simulate the unique "spiking" phenomenon of the FHD system, also known as "Rosensweig instability" or "normal field instability"; see [17, 22, 33]. To do so, we consider a mixture of ferrofluids and the ambient viscous fluids (nonferrofluid) with different viscosities and nearly matching densities. We add the gravity as a forcing





- (a) The implicit-explicit scheme (4.2).
- (b) The developed scheme (3.2)-(3.10).

Fig. 4.3. Energy evolution computed by different time steps, (a) implicit-explicit scheme (4.2), (b) our scheme (3.2)–(3.10).

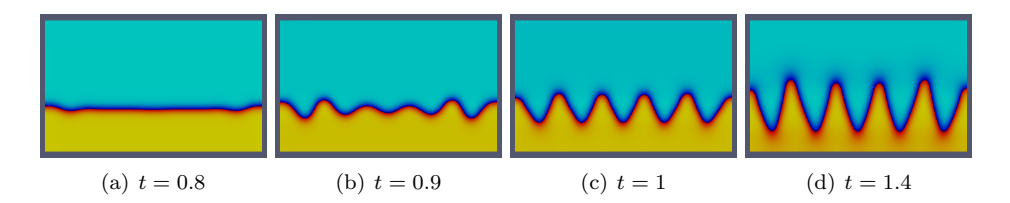


Fig. 4.4. Snapshots of the phase-field variable Φ are taken at various times.

term \boldsymbol{f}_g in the fluid momentum equation (2.5) using the Boussinesq approximation, i.e., $\boldsymbol{f}_g = (1 + \frac{r}{1 + e^{\frac{1-2\Phi}{\epsilon}}})\boldsymbol{g}$, where r is a positive constant that depends on the fluid density, and $|\boldsymbol{g}|$ stands for the magnitude of gravity.

We first carry out the simulations in two dimensional and set the computational domain as $\Omega = [0, 1] \times [0, 0.6]$. The initial conditions are set as

(4.3)
$$u(0, x) = 0, m(0, x) = 0, \Phi(0, x) = \begin{cases} 1, & y \le 0.2, \\ 0, & y > 0.2. \end{cases}$$

The model parameters are set as

$$\left\{ \begin{aligned} \epsilon &= 0.0075, M = 0.0002, \nu_f = 2, \nu_w = 1, \mu = 1, \tau = 1e - 4, \beta = 1, \chi_0 = 0.5, \\ \lambda &= 1, r = 0.1, S = 1, B = \frac{S}{2\epsilon} + 10, \boldsymbol{g} = (0, -6e4), \delta t = 1e - 4, h = \frac{1}{128}. \end{aligned} \right.$$

To generate an analogous uniform applied magnetic field, we set $\mathbf{h}_a = \sum_{s=1}^5 \alpha_s \nabla \phi_s(\mathbf{x})$ by placing five dipoles far distant from the container Ω . The positions \mathbf{x}_s of dipoles are (-0.5, -15), (0, -15), (0.5, -15), (1, -15), and (1.5, -15), and the direction \mathbf{d} of the five dipoles are all (0, 1). The intensities α_s , $s = 1, \ldots, 5$, increase linearly in time, starting from $\alpha_s = 0$ at time t = 0 to maximum value $\alpha_s = 8000$ at time t = 1.6, and from t = 1.6 the intensities are kept constant.

The profiles of the phase-field variable Φ , velocity field \boldsymbol{u} , magnetization \boldsymbol{m} , and effective magnetizing field \boldsymbol{h} are shown in Figures 4.4–4.7, respectively. Under the competition of downward gravity, the upward uniform magnetic field, and the surface tension, the interface profile of the two-phase ferrofluid is unstable and finally forms

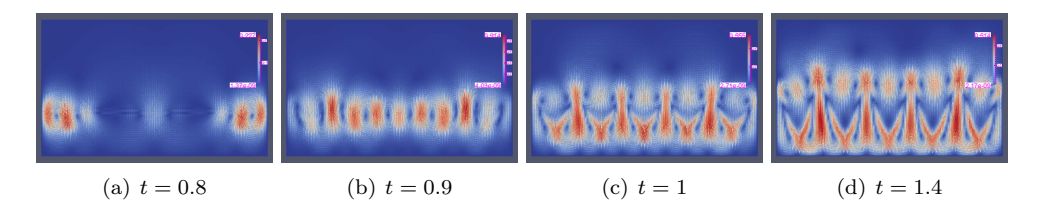


Fig. 4.5. The velocity field u (color represents magnitude, arrows represent vector field) at various times.

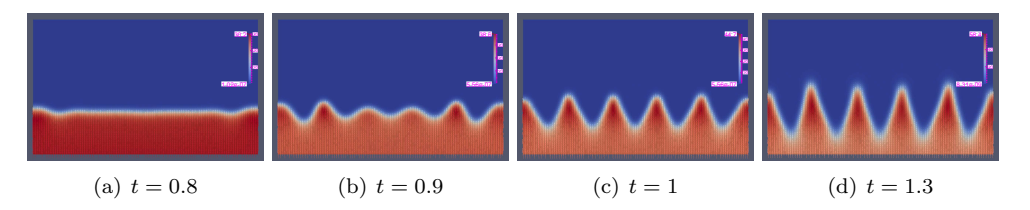


Fig. 4.6. The magnetization field m (color represents magnitude, arrows represent vector field) at t = 0.8, 0.9, 1.0, and 1.3.

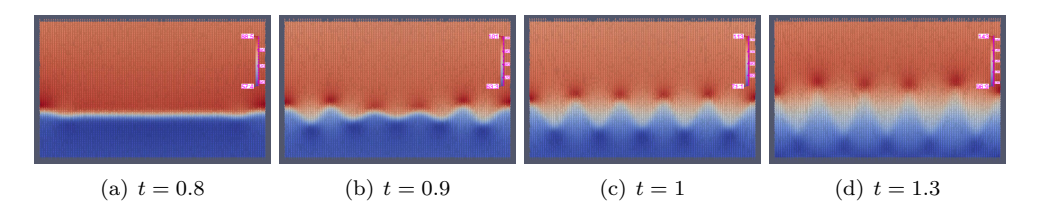


Fig. 4.7. The effective magnetic field h (color represents magnitude, arrows represent vector field) at t = 0.8, 0.9, 1.0, 1.3.

a regular "spiking" or peak-valley steady state. Around t=0.9, six peaks start to appear within the domain and grow over time, shown in Figure 4.4. As the peaks form, the velocity field develops 20 vortices, which are regularly arranged in two layers, shown in Figure 4.5. In Figure 4.6, we find that the ferrofluid is magnetized by the external magnetic field, whereas the magnetization of the nonmagnetic fluid is almost zero. Figure 4.7 shows that the effective magnetic field h exhibits a distinct difference in the region of ferrofluid and nonmagnetic fluid.

We continue to carry out the simulations in three dimensions and set the computational domain as $\Omega = [0,1] \times [0,1] \times [0,\frac{1}{8}]$. The parameters are the same as the 2D simulation. The gravity force imposed in (2.5) takes the same form as the 2D simulations but with $\mathbf{g} = (0,0,-6e4)$. The initial conditions are set as

$$m{u}(0, m{x}) = m{0}, \, m{m}(0, m{x}) = m{0}, \, \Phi(0, m{x}) = egin{cases} 1, & z \leq rac{1}{24}, \\ 0, & z > rac{1}{24}. \end{cases}$$

The analogous uniform applied magnetic field h_a in three dimensions is generated by placing 25 dipoles with $h_a = \sum_{s=1}^{25} \alpha_s \nabla \phi_s(\boldsymbol{x})$, where the direction \boldsymbol{d} of all dipoles is (0,0,1). The positions \boldsymbol{x}_s of dipoles are $(-0.5+0.5i_1,-0.5,-15), (-0.5+0.5i_2,0,-15), (-0.5+0.5i_3,0.5,-15), (-0.5+0.5i_4,1,-15)$, and $(-0.5+0.5i_5,1.5,-15)$ for $i_{1,2,3,4,5} = 0$

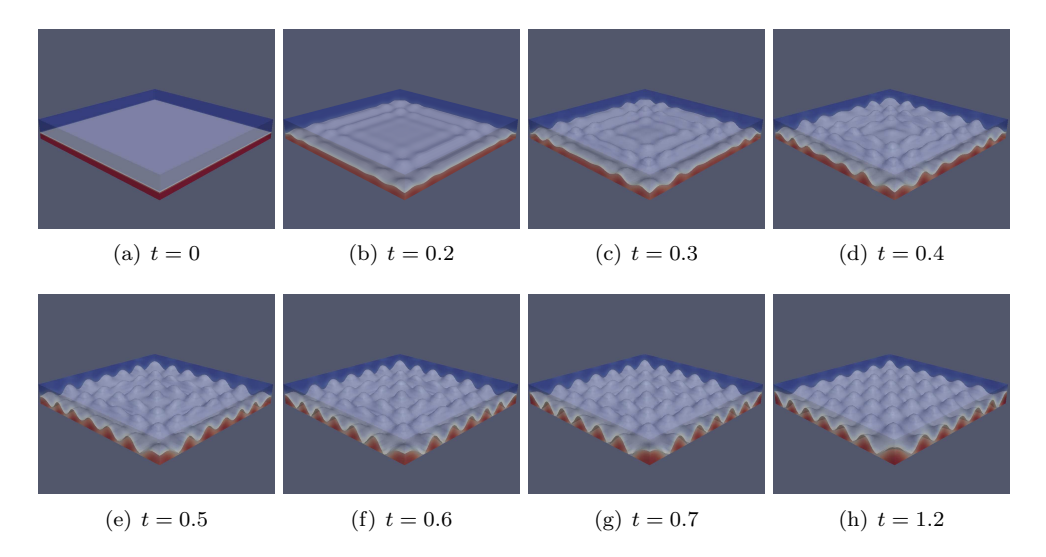


Fig. 4.8. Snapshots of the isosurface of $\{\Phi = 0.5\}$ are taken at various times.

 $0, \ldots, 4$. The intensity is fixed as $\alpha_s = 1000$ for all dipoles. We set $\delta t = 0.001, h = \frac{1}{64}$. The isosurface of the phase-field variable $\{\Phi = 0.5\}$ at various times is shown in Figure 4.8. We observe that some peaks start to appear around t = 0.3. A very regular peak-valley phenomenon is gradually formed over time, which is a typical Rosensweig instability or "spiking" phenomenon of two-phase ferrofluids.

5. Concluding remarks. For the two-phase FHD phase-field model, with the aid of a spatial discretization method using continuous finite elements, this paper aims to construct a numerical scheme with the following desired properties: (i) linearity, (ii) full decoupling, (iii) second-order time accuracy, and (iv) unconditional energy stability. The key technique in the algorithm development is to first use two reconstruction methods, including reforming the magnetostatic equation and introducing a scalar variable based on the "zero-energy-contribution" property, to reformulate the original system into a new but equivalent and algorithmically easy-to-implement system. Several widely used numerical algorithms are then effectively grouped, including the IEQ approach for linearization, the projection methods for fluid equations, the explicit discretization for time marching, etc. The scheme is very efficient, requiring only a few completely independent linear elliptic equations to be solved at each time step. To the best of the authors' knowledge, this is the first fully discrete numerical algorithm that satisfies this many desired properties, especially with a fully decoupled structure for the two-phase FHD phase-field system.

REFERENCES

- S. Afkhami and Y. Renardy, Ferrofluids and magnetically guided superparamagnetic particles in flows: A review of simulations and modeling, J. Engrg. Math., 107 (2017), pp. 231–251.
- [2] G. AKRIVIS, B. LI, AND D. LI, Energy-decaying extrapolated RK-SAV methods for the Allen-Cahn and Cahn-Hilliard equations, SIAM J. Sci. Comput., 41 (2019), pp. A3703-A3727, https://doi.org/10.1137/19M1264412.
- [3] A. BASKARAN, J. S. LOWENGRUB, C. WANG, AND S. M. WISE, Convergence analysis of a second order convex splitting scheme for the modified phase field crystal equation, SIAM J. Numer. Anal., 51 (2013), pp. 2851–2873, https://doi.org/10.1137/120880677.

- [4] S. C. Brenner and L. R. Scott, The Mathematical Theory of Finite Element Methods, 3rd ed., Springer, New York, 2008.
- [5] J. BYROM, P. HAN, M. SAVORY, AND S. L. BISWAL, Directing assembly of DNA-coated colloids with magnetic fields to generate rigid, semiflexible, and flexible chains, Langmuir, 30 (2014), pp. 9045–9052.
- [6] F. CHEN AND J. SHEN, Efficient energy stable schemes with spectral discretization in space for anisotropic cahn-Hilliard systems, Commun. Comput. Phys., 13 (2013), pp. 1189–1208.
- [7] X. Chen, C. Wang, and S. Wise, A preconditioned steepest descent solver for the Cahn-Hilliard equation with variable mobility, Int. J. Numer. Anal. Model., 19 (2022), pp. 839– 863
- [8] K. CHENG, C. WANG, AND S. M. WISE, An energy stable BDF2 fourier pseudo-spectral numerical scheme for the square phase field crystal equation, Commun. Comput. Phys., 26 (2019), pp. 1335–1364.
- [9] Q. Cheng, X. Yang, and J. Shen, Efficient and accurate numerical schemes for a hydrodynamically coupled phase field diblock copolymer model, J. Comput. Phys., 341 (2017), pp. 44–60.
- [10] A. DOAK AND J.-M. VANDEN-BROECK, Travelling wave solutions on an axisymmetric ferrofluid jet, J. Fluid Mech., 865 (2019), pp. 414–439.
- [11] A. S. ELKADY, L. ISKAKOVA, AND A. ZUBAREV, On the self-assembly of net-like nanostructures in ferrofluids, Phys. A, 428 (2015), pp. 257–265.
- [12] J. Fei, S. Xie, and C. Chen, A scalar auxiliary variable (SAV) and operator splitting compact finite difference method for peritectic phase field model, Int. J. Numer. Anal. Model., 19 (2022), pp. 85–100.
- [13] Y. GAO, D. HAN, X. HE, AND U. RÜDE, Unconditionally stable numerical methods for Cahn-Hilliard-Navier-Stokes-Darcy system with different densities and viscosities, J. Comput. Phys., 454 (2022), 110968.
- [14] Y. GAO, X. HE, L. MEI, AND, X. YANG, Decoupled, linear, and energy stable finite element method for the Cahn-Hilliard-Navier-Stokes-Darcy phase field model, SIAM J. Sci. Comput., 40 (2018), pp. B110-B137, https://doi.org/10.1137/16M1100885.
- [15] Y. GAO, X. HE, AND Y. NIE, Second-order, fully decoupled, linearized, and unconditionally stable SAV schemes for Cahn-Hilliard-Darcy system, Numer. Methods Partial Differential Equations, 38 (2022), pp. 1658–1683, https://doi.org/10.1002/num.22829.
- [16] V. GIRAULT AND P. A. RAVIART, Finite Element Method for Navier-Stokes Equations: Theory and Algorithms, Springer-Verlag, Berlin, Heidelberg, 1987, pp. 395–414.
- [17] C. GOLLWITZER, G. MATTHIES, R. RICHTER, I. REHBERG, AND L. TOBISKA, The surface topography of a magnetic fluid: A quantitative comparison between experiment and numerical simulation, J. Fluid Mech., 571 (2007), pp. 455–474.
- [18] J. L. GUERMOND, P. MINEV, AND J. SHEN, An overview of projection methods for incompressible flows, Comput. Methods Appl. Mech. Engrg., 195 (2006), pp. 6011–6045.
- [19] P. GUYENNE AND E. I. PARAU, An operator expansion method for computing nonlinear surface waves on a ferrofluid jet, J. Comput. Phys., 321 (2016), pp. 414–434.
- [20] D. Han, A decoupled unconditionally stable numerical scheme for the Cahn-Hilliard-Hele-Shaw system, J. Sci. Comput., 66 (2016), pp. 1102–1121, https://doi.org/10.1007/s10915-015-0055-v.
- [21] D. HAN AND X. WANG, A second order in time, uniquely solvable, unconditionally stable numerical scheme for Cahn-Hilliard-Navier-Stokes equation, J. Comput. Phys., 290 (2015), pp. 139–156, https://doi.org/10.1016/j.jcp.2015.02.046.
- [22] Y. Hu, D. Li, And X. Niu, Phase-field-based lattice Boltzmann model for multiphase ferrofluid flows, Phys. Rev. E (3), 98 (2018), 033301.
- [23] Q. Huang, X. Yang, and X. He, Numerical approximations for a smectic-A liquid crystal flow model: First-order, linear, decoupled and energy stable schemes, Discrete Contin. Dyn. Syst. Ser. B, 23 (2018), pp. 2177-2192.
- [24] D. KAY, V. STYLES AND R. WELFORD, Finite element approximation of a Cahn-Hilliard-Navier-Stokes system, Interface Free Bound., 10 (2008), pp. 15–43.
- [25] J. KOU, S. SUN, AND X. WANG, Linearly decoupled energy-stable numerical methods for multicomponent two-phase compressible flow, SIAM J. Numer. Anal., 56 (2018), pp. 3219–3248, https://doi.org/10.1137/17M1162287.
- [26] R. LI, Y. GAO, J. CHEN, L. ZHANG, X. HE, AND Z. CHEN, Discontinuous finite volume element method for a coupled Navier-Stokes-Cahn-Hilliard phase field model, Adv. Comput. Math., 46 (2020), 25.
- [27] L. LIANG, J. ZHU, AND X. XUAN, Three-dimensional diamagnetic particle deflection in ferrofluid microchannel flows, Biomicrofluidics, 5 (2011), 034110.

- [28] F. Lin, X. He, and X. Wen, Fast, unconditionally energy stable large time stepping method for a new Allen-Cahn type square phase-field crystal model, Appl. Math. Lett., 92 (2019), pp. 248–255.
- [29] C. LIU AND J. SHEN, A phase field model for the mixture of two incompressible fluids and its approximation by a Fourier-spectral method, Phys. D, 179 (2003), pp. 211–228.
- [30] T. LIU, J. WU, C. XIA, AND Z. QIAN, A microvalve driven by a ferrofluid-based actuator, in Advanced Materials Research, Vols. 433–440, Trans Tech Publications, Stafa-Zurich, Switzerland, 2012, pp. 3767–3772.
- [31] O. T. MEFFORD, R. C. WOODWARD, J. D. GOFF, T. P. VADALA, T. G. S. PIERRE, J. P. DAILEY, AND J. S. RIFFLE, Field-induced motion of ferrofluids through immiscible viscous media: Testbed for restorative treatment of retinal detachment, J. Magn. Magn. Mater., 311 (2007), pp. 347–353.
- [32] N.-T. NGUYEN, Micro-magnetofluidics: Interactions between magnetism and fluid flow on the microscale, Microfluid Nanofluidics, 12 (2012), pp. 1–16.
- [33] R. H. NOCHETTO, A. J. SALGADO, AND I. TOMAS, A diffuse interface model for two-phase ferrofluid flows, Comput. Methods Appl. Mech. Engrg., 309 (2016), pp. 497–531.
- [34] S. Pal, A. Datta, S. Sen, A. Mukhopdhyay, K. Bandopadhyay, and R. Ganguly, Characterization of a ferrofluid-based thermomagnetic pump for microfluidic applications, J. Magn. Magn. Mater., 323 (2011), pp. 2701–2709.
- [35] Z. Qiao, S. Sun, T. Zhang, and Y. Zhang, A new multi-component diffuse interface model with Peng-Robinson equation of state and its scalar auxiliary variable (SAV) approach, Commun. Comput. Phys., 26 (2019), pp. 1597–1616.
- [36] Y. Qin, C. Wang, and Z. Zhang, A positivity-preserving and convergent numerical scheme for the binary fluid-surfactant system, Int. J. Numer. Anal. Model., 18 (2021), pp. 399–425.
- [37] R. E. ROSENSWEIG, Ferrohydrodynamics, Cambridge University Press, Cambridge, UK, 1985.
- [38] R. E. ROSENSWEIG, Magnetic fluids, Annu. Rev. Fluid Mech., 19 (1987), pp. 437–461.
- [39] J. Shen, On error estimates of projection methods for the Navier-Stokes equations: Second-order schemes, Math. Comp., 65 (1996), pp. 1039–1065.
- [40] J. SHEN, C. WANG, X. WANG, AND S. M. WISE, Second-order convex splitting schemes for gradient flows with Ehrlich-Schwoebel type energy: Application to thin film epitaxy, SIAM J. Numer. Anal., 50 (2012), pp. 105-125, https://doi.org/10.1137/110822839.
- [41] J. SHEN, J. XU, AND J. YANG, A new class of efficient and robust energy stable schemes for gradient flows, SIAM Rev., 61 (2019), pp. 474-506, https://doi.org/10.1137/17M1150153.
- [42] J. SHEN AND X. YANG, Numerical approximations of Allen-Cahn and Cahn-Hilliard equations, Discrete Contin. Dyn. Syst., 28 (2010), pp. 1669–1691.
- [43] J. Shen and X. Yang, Decoupled energy stable schemes for phase-field models of two phase complex fluids, SIAM J. Sci. Comput., 36 (2014), pp. B122-B145, https://doi.org/10.1137/130921593.
- [44] J. Shen and X. Yang, Decoupled, energy stable schemes for phase-field models of two-phase incompressible flows, SIAM J. Numer. Anal., 53 (2015), pp. 279–296, https://doi.org/10.1137/140971154.
- [45] J. SHEN AND X. YANG, The IEQ and SAV approaches and their extensions for a class of highly nonlinear gradient flow systems, in 75 Years of Mathematics of Computation, Contemp. Math., 754 AMS, Providence, RI, 2020, pp. 217–245.
- [46] Y. SHIBATA, T. TAKAMINE, AND M. KAWAJI, Emission of liquid droplets from an interface of bidrops pulled by a ferrofluid in a microchannel, Int J. Therm. Sci., 50 (2011), pp. 233–238.
- [47] A. I. M. SHINKAI, H. HONDA, AND T. KOBAYASHI, Medical application of functionalized magnetic nanoparticles, J. Biosci. Bioeng., 100 (2005), pp. 1–11.
- [48] M. I. Shliomis, Effective viscosity of magnetic suspensions, Sov. phys. JETP, 34 (1972), pp. 1291–1294.
- [49] M. I. Shliomis, Ferrohydrodynamics: Retrospective and issues, in Ferrofluids, Lect. Notes Phys. 594, Springer, Berlin, Heidelberg, 2002, pp. 85–111.
- [50] A. VINOGRADOVA, V. TURKOV, AND V. NALETOVA, Modeling of ferrofluid-based microvalves in the magnetic field created by a current-carrying wire, J. Magn. Magn. Mater., 470 (2019), pp. 18–21.
- [51] C. Xu, C. Chen, X. Yang, and X. He, Numerical approximations for the hydrodynamics coupled binary surfactant phase field model: Second order, linear, unconditionally energy stable schemes, Commun. Math. Sci., 17 (2019), pp. 835–858.
- [52] Y. YAN, W. CHEN, C. WANG, AND S. M. WISE, A second-order energy stable BDF numerical scheme for the Cahn-Hilliard equation, Commun. Comput. Phys., 23 (2018), pp. 572–602.
- [53] J. YANG, S. MAO, X. HE, X. YANG, AND Y. HE, A diffuse interface model and semi-implicit energy stable finite element method for two-phase magnetohydrodynamic flows, Comput. Methods Appl. Mech. Engrg., 356 (2019), pp. 435–464.

- [54] X. Yang, A novel fully-decoupled, second-order time-accurate, unconditionally energy stable scheme for a flow-coupled volume-conserved phase-field elastic bending energy model, J. Comput. Phys., 432 (2021), 110015.
- [55] X. Yang, On a novel fully decoupled, second-order accurate energy stable numerical scheme for a binary fluid-surfactant phase-field model, SIAM J. Sci. Comput., 43 (2021), pp. B479–B507, https://doi.org/10.1137/20M1336734.
- [56] X. Yang and X. He, A fully-discrete decoupled finite element method for the conserved Allen-Cahn type phase-field model of three-phase fluid flow system, Comput. Methods Appl. Mech. Engrg., 389 (2022), 114376.
- [57] X. Yang and X. He, Numerical approximations of flow coupled binary phase field crystal system: Fully discrete finite element scheme with second-order temporal accuracy and decoupling structure, J. Comput. Phys., 467 (2022), 111448.
- [58] X. Yang and L. Ju, Linear and unconditionally energy stable schemes for the binary fluidsurfactant phase field model, Comput. Methods Appl. Mech. Engrg., 318 (2017), pp. 1005– 1029.
- [59] X. Yang and H. Yu, Efficient second order unconditionally stable schemes for a phase field moving contact line model using an invariant energy quadratization approach, SIAM J. Sci. Comput., 40 (2018), pp. B889–B914, https://doi.org/10.1137/17M1125005.
- [60] X. Yang and G. D. Zhang, Convergence analysis for the invariant energy quadratization (IEQ) schemes for solving the Cahn-Hilliard and Allen-Cahn equations with general nonlinear potential, J. Sci. Comput., 82 (2020), pp. 1–28.
- [61] X. Yang, J. Zhao, and X. He, Linear, second order and unconditionally energy stable schemes for the viscous Cahn-Hilliard equation with hyperbolic relaxation using the invariant energy quadratization method, J. Comput. Appl. Math., 343 (2018), pp. 80-97.
- [62] P. Yue, J. Feng, C. Liu, and J. Shen, A diffuse-interface method for simulating two-phase flows of complex fluids, J. Fluid Mech., 515 (2005), pp. 293–317.
- [63] J. Zeng, Y. Deng, P. Vedantam, T. R. Tzeng, and X. Xuan, Magnetic separation of particles and cells in ferrofluid flow through a straight microchannel using two offset magnets, J. Magn. Magn. Mater., 346 (2013), pp. 118–123.
- [64] G. Zhang, X. He, and X. Yang, A fully decoupled linearized finite element method with second-order temporal accuracy and unconditional energy stability for incompressible MHD equations, J. Comput. Phys., 448 (2022), 110752.
- [65] G.-D. Zhang, X. He, and X. Yang, Decoupled, linear, and unconditionally energy stable fully discrete finite element numerical scheme for a two-phase ferrohydrodynamics model, SIAM J. Sci. Comput., 43 (2021), pp. B167–B193, https://doi.org/10.1137/19M1288280.
- [66] H. ZHANG, X. YANG, AND J. ZHANG, Stabilized invariant energy quadratization (S-IEQ) method for the molecular beam epitaxial model without slope section, Int. J. Numer. Anal. Model., 18 (2021), pp. 642–655.
- [67] J. Zhao, X. Yang, Y. Gong, and Q. Wang, A novel linear second order unconditionally energy stable scheme for a hydrodynamic Q-tensor model of liquid crystals, Comput. Methods Appl. Mech. Engrg., 318 (2017), pp. 803–825.